ACCOUNTS of chemical research

pubs.acs.org/accounts
Article

Organic Photocatalyst Utilizing Triplet Excited States for Highly Efficient Visible-Light-Driven Polymerizations

Yonghwan Kwon, Woojin Jeon, Johannes Gierschner,* and Min Sang Kwon*

Cite This: *Acc. Chem. Res.* 2025, 58, 1581−1595
Read Online

CONSPECTUS: Ultraviolet (UV) light has traditionally been used to drive photochemical organic transformations, mainly due to the limited visible-light absorption of most organic molecules. However, the high energy associated with UV light often causes undesirable side reactions. In the late 2000s, MacMillan, Yoon, and Stephenson pioneered the use of visible light in conjunction with photocatalysts (PCs) to initiate organic transformations. This innovative approach overcame the limitations of UV light by utilizing visible-light-absorbing PCs in their photoexcited states for electron or energy transfer, generating reactive radical species and promoting the photoreactions. Furthermore, while the photocatalysis has predominantly relied on transition-metal complexes, concerns over the potential toxicity, cost, and sustainability of these metals have driven the development of organic PCs. These organic PCs eliminate the need for metal removal, offer structural diversity, and enable tuning of their properties, thus paving the way for the creation of a tailored library of PCs.

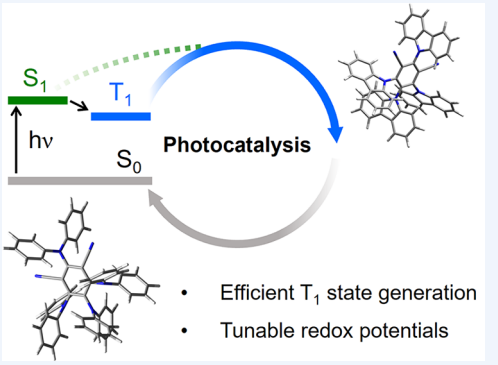

In recent decades, significant advancements have been made in the development of novel organic PCs with diverse scaffolds, with a notable example being the work of Zhang et al. in 2016. They demonstrated that cyanoarene analogues, originally developed by Adachi et al. for thermally activated delayed fluorescence (TADF) in organic light-emitting diodes, could function effectively as PCs. Building on these insights, we developed a PC design platform featuring TADF compounds with twisted donor−acceptor structures, which paved the way for new PC discoveries. We showcased these PCs' ability (i) to generate long-lived lowest triplet excited (T_1) states and (ii) to tune redox potentials by independently modifying donor and acceptor moieties. Through this platform, we discovered PCs with varying redox potentials and the capability to effectively populate T_1 states, establishing structure−property relationships within our PC library and creating PC selection criteria for targeted reactions. Specifically, we tailored PCs for highly efficient reversible-deactivation radical polymerizations, including organocatalyzed atom transfer radical polymerization, photoinduced electron/energy transfer reversible addition−fragmentation chain transfer polymerization, and atom transfer radical polymerization with dual photoredox/copper catalysis as well as rapid free radical polymerizations. These advancements have also facilitated the development of functionalized, visible-light-cured adhesives for advanced display technologies. Furthermore, we investigated the origins of the exceptional catalytic performance of these PCs through comprehensive mechanistic studies, including electrochemical and photophysical measurements, quantum chemical calculations, and kinetics simulations. Specifically, we studied the formation and degradation of key PC intermediates in photocatalytic dehalogenations of alkyl and aryl halides. Our findings revealed a distinctive photodegradation pattern in the cyanoarene-based PCs, which significantly impact their catalytic efficiency in the reaction. Additionally, this discovery led us to introduce a concept of beneficial PC degradation for the first time.

Over the past decades, organic photocatalysis based on the T_1 state has become central to polymerization and organic synthesis. Utilizing our PC design platform, we have developed novel PCs and catalytic systems that enhance the overall efficiency of various organic transformations. In this overview of our contributions to visible-light-driven organic photocatalysis, we highlight the role of the T_1 state in broadening applications through mechanistic analysis, enabling more sustainable transformations.

KEY REFERENCES

- Singh, V. K.; Yu, C.; Badgujar, S.; Kim, Y.; Kwon, Y.; Kim, D.; Lee, J.; Akhter, T.; Thangavel, G.; Park, L. S.; Lee, J.; Nandajan, P. C.; Wannemacher, R.; Milián-Medina, B.; Lüer, L.; Kim, K. S.; Gierschner, J.; Kwon, M. S. Highly Efficient Organic Photocatalysts Discovered via a Computer-Aided-Design Strategy for Visible-

Received: January 5, 2025
Revised: April 16, 2025
Accepted: April 17, 2025
Published: May 1, 2025

https://doi.org/10.1021/acs.accounts.4c00847
Acc. Chem. Res. 2025, 58, 1581−1595

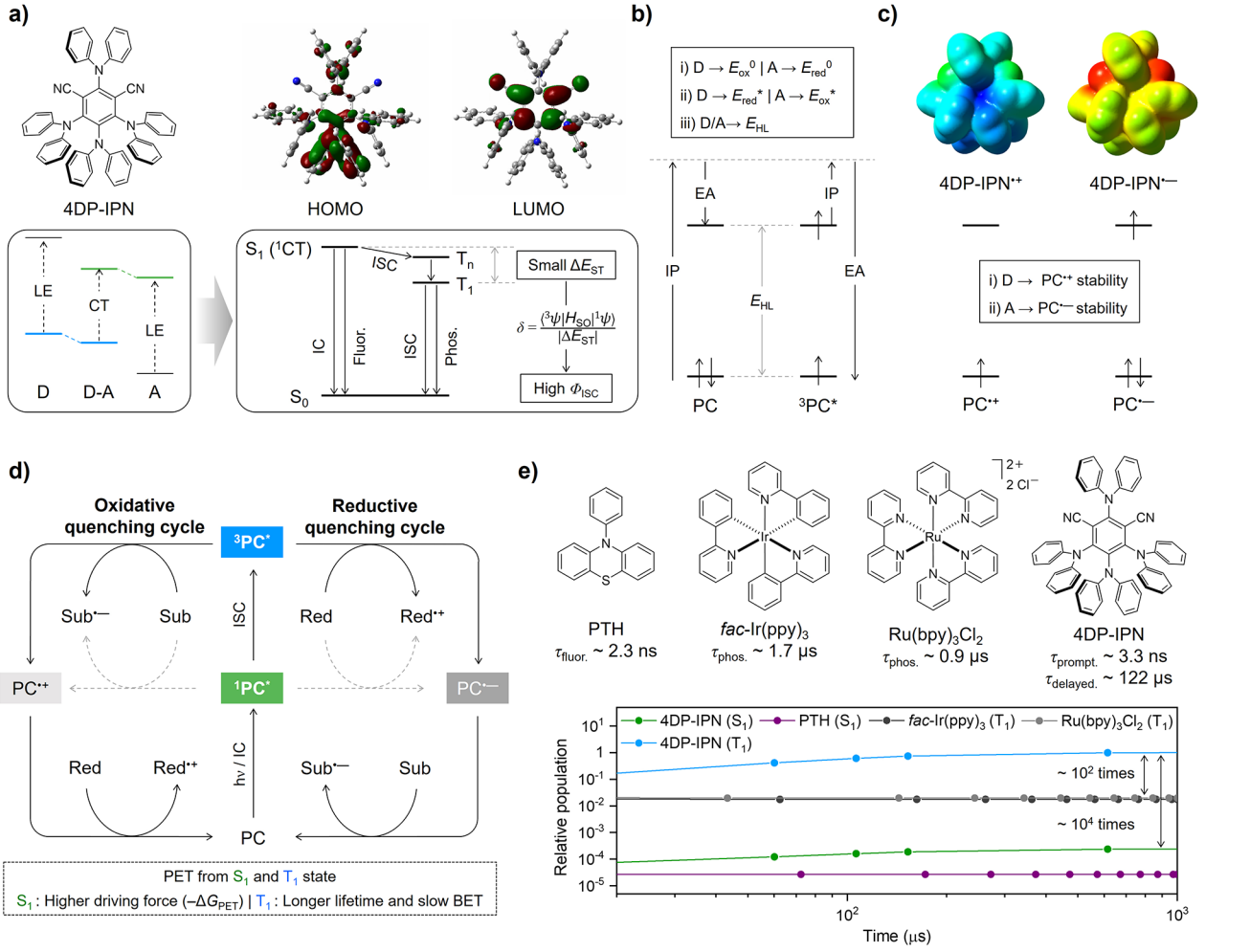

Figure 1. (a) Schematic energy and Jablonski diagrams of strongly twisted donor−acceptor compounds. Calculated HOMO and LUMO topologies of 4DP-IPN are shown (top). D, donor moiety; A, acceptor moiety; LE, locally excited; CT, charge-transfer; IC, internal conversion; Flour., fluorescence; ISC, intersystem crossing; Phos., phosphorescence; ΔE_{ST}, energy gap between singlet and triplet states; δ, first-order mixing coefficient between singlet and triplet states; $^1\Psi$, singlet wave functions; $^3\Psi$, triplet wave functions; H_{SO}, spin−orbit Hamiltonian; Φ_{ISC}, the quantum yield of ISC. (b) PC design principles for tuning the light absorption and redox potentials of ground- and excited-state correlated with electron affinity (EA) and ionization potential (IP). (c) Stability control of PC intermediates in the PC cycle, with exemplified electrostatic potential maps of 4DP-IPN$^{\bullet+}$ and 4DP-IPN$^{\bullet-}$ (top). (d) General photoredox catalysis mechanism. (e) Relative populations of S_1 and T_1 states of 4DP-IPN, compared with those of the representative PCs, based on kinetic simulations.[4]

Light-Driven Atom Transfer Radical Polymerization. *Nat. Catal.* **2018**, *1*, 794−804.[1] A pioneering investigation into PC design principles based on a strongly twisted donor−acceptor structure, enabling efficient generation of T_1 states and tunable redox potentials. Furthermore, we demonstrated highly efficient O-ATRP using PCs systematically discovered through our design strategy.

- Lee, Y.; Kwon, Y.; Kim, Y.; Yu, C.; Feng, S.; Park, J.; Doh, J.; Wannemacher, R.; Koo, B.; Gierschner, J.; Kwon, M. S. A Water-Soluble Organic Photocatalyst Discovered for Highly Efficient Additive-Free Visible-Light-Driven Grafting of Polymers from Proteins at Ambient and Aqueous Environments. *Adv. Mater.* **2022**, *34*, 2108446.[2] This contribution presented a new approach to achieving water-soluble PCs based on the PC design principles. Utilizing the water-soluble PC, we demonstrated highly efficient visible-light-driven oxygen-tolerant PET-RAFT polymerization for protein−polymer conjugates in an aqueous medium.

- Jeon, W.; Kwon, Y.; Kwon, M. S. Highly Efficient Dual Photoredox/Copper Catalyzed Atom Transfer Radical Polymerization Achieved through Mechanism-Driven Photocatalyst Design. *Nat. Commun.* **2024**, *15*, 5160.[3] This contribution highlighted the importance of detailed mechanistic investigations in the PC design. Utilizing PCs that can be efficiently regenerated within the PC cycle, we achieved highly efficient ATRP with dual photoredox/copper catalysis with ppb-level PC loading.

- Kwon, Y.; Lee, J.; Noh, Y.; Kim, D.; Lee, Y.; Yu, C.; Roldao, J. C.; Feng, S.; Gierschner, J.; Wannemacher, R.; Kwon, M. S. Formation and Degradation of Strongly Reducing Cyanoarene-Based Radical Anions towards Efficient Radical Anion-Mediated Photoredox Catalysis. *Nat. Commun.* **2023**, *14*, 92.[4] This contribution investigated underlying principles behind formation of radical anions in the cyanoarene-based PCs, where the T_1 state plays a key role. Furthermore, degradation behaviors of cyanoarenes determining overall efficiency

https://doi.org/10.1021/acs.accounts.4c00847
Acc. Chem. Res. 2025, 58, 1581−1595

of photocatalysis were discussed in relation to competitive electron transfer.

- Kwon, Y.; Lee, S.; Kim, J.; Jun, J.; Jeon, W.; Park, Y.; Kim, H. J.; Gierschner, J.; Lee, J.; Kim, Y.; Kwon, M. S. Ultraviolet Light Blocking Optically Clear Adhesives for Foldable Displays via Highly Efficient Visible-Light Curing. *Nat. Commun.* **2024**, *15*, 2829.[5] This contribution underscored the necessity of in-depth mechanistic studies to clarify the interactions between PC and additives. Through this investigation, we developed a new photoinitiating system that enables a highly rapid polymerization to produce UV-blocking OCA film.

1. INTRODUCTION

Photochemical organic transformations have traditionally relied on ultraviolet (UV) light, primarily due to the limited visible-light absorption of most organic molecules, so that visible-light-driven photochemical processes were little explored.[6,7] However, the high energy of UV light often leads to undesired side reactions and low selectivity, restricting the scope of photochemical reactions. To overcome this limitation, MacMillan, Stephenson, and Yoon pioneered the field of "visible-light-driven photocatalysis" in the late 2000s.[6−10] They demonstrated that, in the presence of photocatalysts (PCs) that absorb visible light, these catalytic reactions can achieve high selectivity and minimal side reactions under mild conditions. This breakthrough enabled integrations of photocatalysis with various other catalytic methods,[8,11−18] facilitating the development of novel synthetic protocols.

Organic PCs can populate both the lowest singlet (S_1) and triplet (T_1) excited states after light absorption (Figure 1d). Therefore, the contribution of each excited state to photoredox-mediated reactions remains a topic of ongoing debate.[19] Among these states, PCs in the S_1 state (^{1}PC*) have a higher energy, which allows for a faster photoinduced electron transfer (PET) rate constant (k_{PET}) compared with that of PCs in the T_1 state (^{3}PC*), due to a larger driving force for PET ($-\Delta G_{PET}$) of the former. However, because ^{1}PC* has a relatively short excited-state lifetime, a relatively large amount of PC or high substrate concentration is required to ensure effective bimolecular collisions. This results in increased absorbance of the reaction mixture, which inhibits effective light penetration into the reaction center (inner filter effect),[20] and requires postreaction processes to remove PC residues in the product, thereby increasing the overall process costs during scale-up. Contrary, the ^{3}PC* benefits from a significantly longer lifetime due to its spin-forbidden nature. This is particularly evident in organic PCs, which, lacking heavy-metal atoms, typically have much longer T_1 state lifetimes (in the millisecond range) compared with those of their organometallic counterparts (in the microsecond range). This extended lifetime increases the effective concentration of ^{3}PC* in the photostationary state, thereby enhancing the overall rate of the photocatalytic process. For instance, the prolonged lifetime enables a rapid overall PET rate (ν_{PET}, M s^{-1}) with the substrate, given by

$$\nu_{PET} = k_{PET}[PC^*][Sub] \quad (1)$$

where [PC*] and [Sub] correspond to the concentrations of PC* and the substrate, respectively. This role of the T_1 state becomes even more critical in polymerizations, where the increasing viscosity hinders the bimolecular collisions between PC* and the substrate.[21] In addition, slow back-ET (BET) process, which involves a spin-flip within a triplet contact radical ion pair, enhances the ET efficiency.[22] These characteristics of the T_1 state lead to a more efficient photoredox catalytic process, reduce the required PC loading, simplify postreaction purification, and enable bulk scalability. Thus, based on these benefits, ^{3}PC* in photocatalytic reactions has been extensively studied in the organic transformations.[23,24]

However, generation of these T_1 states in all organic molecules via intersystem crossing (ISC) from the S_1 state is typically challenging due to the small spin−orbit coupling, a result of the absence of heavy atoms. In recent years, advances in synthetic protocols have led to significant progress in development of organic emitters that exploit T_1 states. Since 2010, these efforts have led to the development of a wide range of organic light emitters with long excited-state lifetimes, based on room-temperature phosphorescence[25] and thermally activated delayed fluorescence (TADF),[26] the latter relying on reverse ISC (RISC) from T_1 to S_1 state.[27] Since the mid-2010s, there have been several attempts to utilize these emitters as PCs, opening new avenues in organic photocatalysis.[28,29] A notable example is Zhang's demonstration in 2016, which employed cyanoarenes—originally developed by Adachi et al. as TADF compounds for organic light emitting diodes.[30]

To drive efficient PET-driven reactions, the standard reduction potential relationship between the PC and a target substrate is a key factor. For example, for the efficient reductive quenching system (Figure 1d), the excited-state reduction potential of PC (E_{red}*(PC)) should be more positive than the ground-state oxidation potential of a reductant (E_{ox}^0(Red)), while the ground-state reduction potential of PC (E_{red}^0(PC)) should be more negative than that of the target substrate (E_{red}^0(Sub)), as described by

$$-\Delta G_{PET} = \mathcal{F}(E_{red}^*(PC) - E_{ox}^0(Red))$$

for opening the reductive quenching cycle (2)

$$-\Delta G_{ET} = \mathcal{F}(E_{red}^0(Sub) - E_{red}^0(PC))$$

for closing the reductive quenching cycle (3)

where F denotes Faraday constant. Additionally, several additional PC's properties must be controlled to facilitate efficient photocatalysis, including the light absorption at appropriate wavelengths, and the energies and lifetimes of the S_1 and T_1 states. Traditionally, unbiased screening has been employed to identify efficient PCs with the desired catalytic properties for specific reactions. However, this trial-and-error approach is often time-consuming and costly. Therefore, a systematic approach to PC discovery is necessary to identify suitable PCs more efficiently.[24,31]

Building on the aforementioned insights which Adachi and Zhang proposed, we developed a PC design platform based on TADF compounds with twisted donor−acceptor structures, paving the way for new PC discoveries (Figure 1a).[1] Specifically, we demonstrated that these PCs could generate long-lived T_1 states while also enabling to tune their redox potentials of PC intermediates though donor and acceptor modifications (Figure 1b and 1c). Utilizing our PC platform, we screened PCs with varying redox potentials and T_1 state generation efficiencies, to establish structure−property rela-

https://doi.org/10.1021/acs.accounts.4c00847
Acc. Chem. Res. 2025, 58, 1581−1595

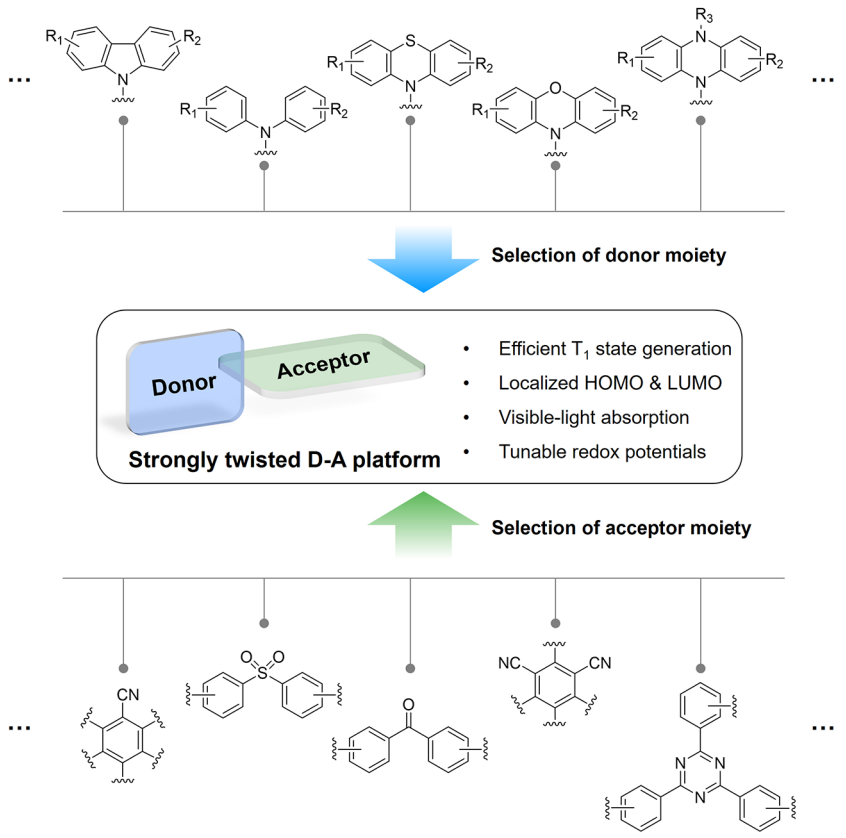

Figure 2. Schematic representation of the strongly twisted donor–acceptor PC design platform.

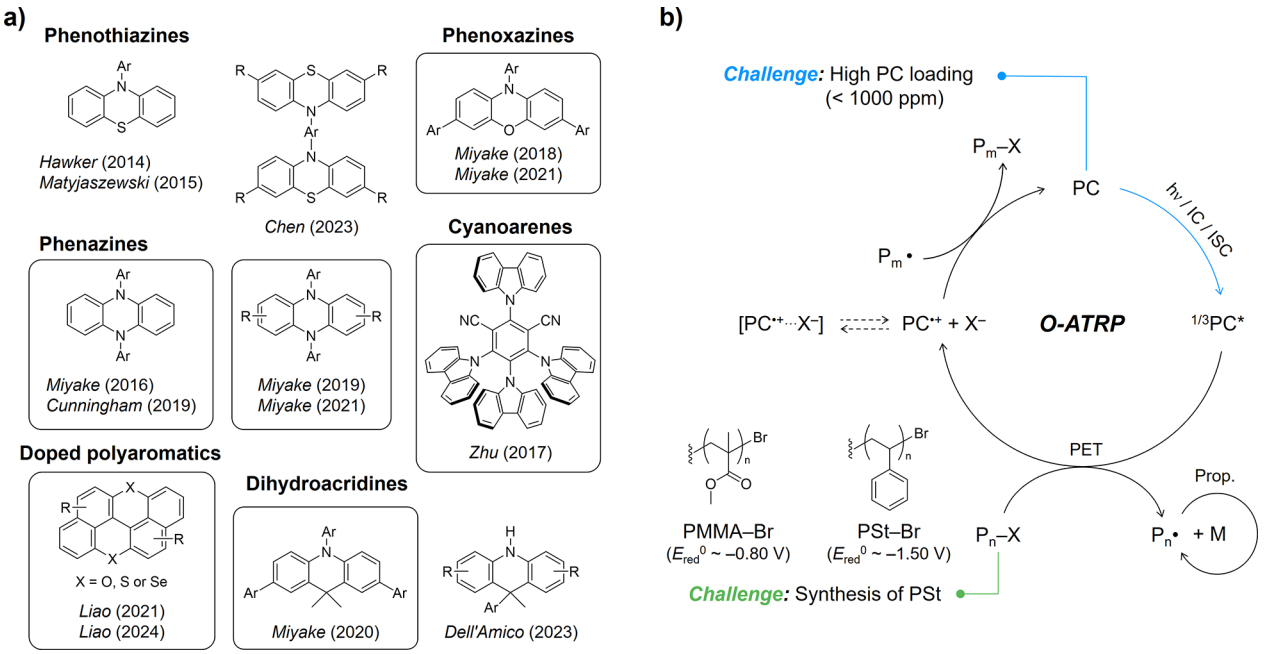

Figure 3. (a) Previously reported PC library for O-ATRP. PCs reported to utilize the T_1 state are highlighted in the box. (b) Proposed mechanism of O-ATRP and key challenges to be addressed.

tionships within our PC library and to formulate PC selection criteria, and identify efficient PCs for reversible-deactivation radical polymerizations (RDRPs); this included organocatalyzed atom transfer radical polymerization (O-ATRP),[1] photoinduced electron/energy transfer reversible addition–fragmentation chain transfer (PET-RAFT) polymerization,[2,32] and ATRP with dual photoredox/copper catalysis,[3] as well as rapid free radical polymerizations (Figure 2).[5,33−35] Furthermore, we investigated origins of the exceptional catalytic performance of these PCs through in-depth mechanistic studies, including electrochemical and photophysical measurements, quantum chemical calculations, and kinetic simulations.

https://doi.org/10.1021/acs.accounts.4c00847
Acc. Chem. Res. 2025, 58, 1581−1595

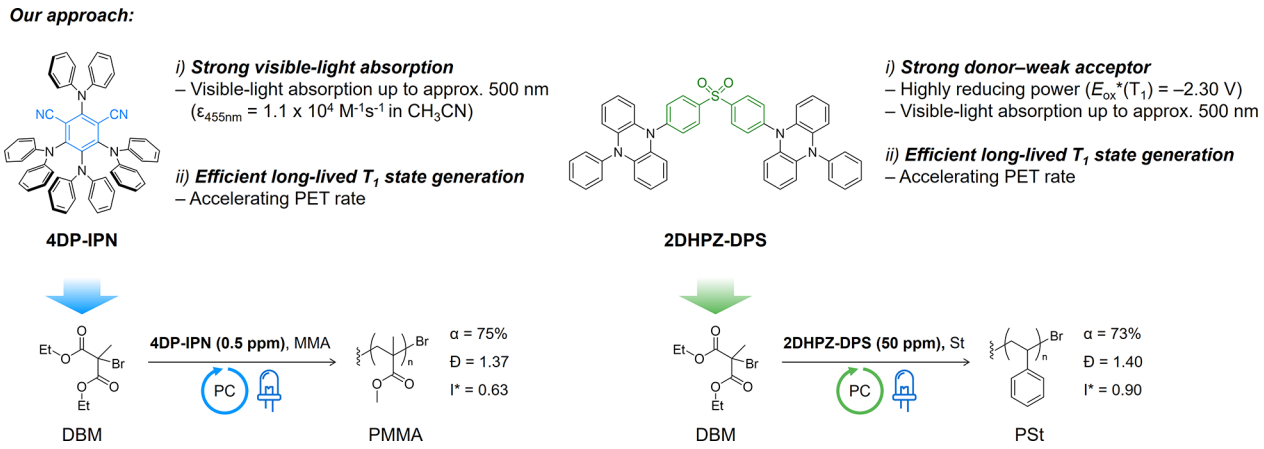

Figure 4. PC design strategies for addressing challenges in O-ATRP using 4DP-IPN and 2DHPZ-DPS.

Specifically, we examined formations and degradations of key PC intermediates in photocatalytic dehalogenations of alkyl and aryl halides.[4] Our research revealed a unique photodegradation pattern in cyanoarene-based PCs, which had a significant impact on the overall reaction efficiency. Notably, this led us to establish for the first time a concept of beneficial PC degradation.[36]

From the early stages of investigations on the organic PCs utilizing T_1 states, we have made contributions to their developments and their applications in polymerizations. In this *Account*, we summarize our key findings and highlight major discoveries in the field, including those beyond our own work, offering readers a comprehensive perspective on past developments, the current state of research, and future directions.

2. OPENING THE PHOTOCATALYTIC CYCLE VIA THE TRIPLET EXCITED STATE

2.1. O-ATRP

Photoredox-mediated ATRP, first pioneered by Hawker et al.,[37,38] provides a strategy for activating alkyl halide initiators through an outer-sphere ET, enabling a synthesis of well-controlled polymers. Since then, numerous groups have worked on the development of purely organic PCs that combine visible-light absorption with the utilization of ^{3}PC* (Figure 3a). Following the successful synthesis of poly(methyl methacrylate) (PMMA) reported by Miyake et al.,[39,40] significant advancements have been made using various molecular scaffolds, including phenothiazines,[41,42] phenoxazines,[43−45] phenazines,[46−48] dihydroacridines,[49,50] cyanoarenes,[1,51] and doped polyaromatic frameworks.[52,53]

Despite the advancements in O-ATRP, PC loadings remain relatively high (approximately 1000 parts per million (ppm)). We envisioned that the maximized population of T_1 state can address this limitation enabling initiator activation with lower PC loading. Among our PC library, we noticed that 4DP-IPN, a cyanoarene substituted with diphenylamine, reaches the photostationary state where the T_1 state population is approximately two orders of magnitude higher than those of Ir(III) or Ru(II) complexes,[4] owing to its extended T_1 state lifetime (Figure 1e). Thus, we anticipated that 4DP-IPN would be a promising PC for O-ATRP (Figure 4, left) due to its superior properties to enhance the PET efficiency, including: (i) strong visible-light absorption, (ii) highly efficient generation of a long-lived T_1 state (Φ_{ISC} = 84% and $\tau_{delayed.}$ > 100 μs),[4] (iii) appropriate redox potentials for the PC cycle, and (iv) high radical cation stability. Consequently, we demonstrated that 4DP-IPN allowed for a significant reduction in PC loading in O-ATRP, reaching sub-ppm levels as low as 0.5 ppm for PMMA synthesis. This ultralow PC loading eliminates the need for additional purification processes. Meanwhile, O-ATRP presents additional challenges, particularly in the synthesis of polystyrene (PSt). Compared with MMA (E_{red}^0 (PMMA−Br) ≈ −0.80 V), the end-group in PSt has a much more negative E_{red}^0 (E_{red}^0 (PSt−Br) ≈ −1.50 V), making PSt-Br activation more challenging. To address this, we prepared a diphenylsulfone-based PC, 2DHPZ-DPS (Figure 4, right), in which the diphenylsulfone ($EA_{calc.}$ = 1.82 eV) is a weaker acceptor than isophthalonitrile ($EA_{calc.}$ = 2.26 eV).[1] This increases the lowest unoccupied molecular orbital (LUMO) energy within the donor−acceptor structure, enhancing its reducing power (E_{ox}* = −2.30 V) compared to that of 4DP-IPN (E_{ox}* = −1.41 V).[1] Consequently, utilizing the reducing power of 2DHPZ-DPS to activate PSt-Br and its long-lived T_1 state ($\tau_{delayed.}$ > 1.0 ms), we synthesized PSt with high yields (60−70%). However, the PC loading for PSt remained high at 50 ppm, and the molecular weight (MW) distribution was still broad (Đ = 1.40). Therefore, further investigations are required to achieve the well-controlled synthesis of PSt.

2.2. PET-RAFT Polymerization

Recognizing the feasibility of cyanoarenes in O-ATRP, we extended their application to another RDRP method, PET-RAFT polymerization. PET-RAFT polymerization is one of the most extensively studied fields of RDRP, combining photocatalysis and RAFT polymerization. In 2014, Boyer implemented PET-RAFT polymerization using an Ir(III) complex as PC without an external radical source, unlike the conventional RAFT polymerization.[54] Since then, PET-RAFT has evolved to incorporate purely organic PCs, where the T_1 state primarily drives the reaction.[55,56] Building on these advances, in 2019, we demonstrated a highly efficient, visible-light-driven oxygen-tolerant PET-RAFT utilizing 4DP-IPN.[32] Based on the strong visible-light absorption and efficient T_1 state generation of 4DP-IPN, we achieved low PC loadings of 5 ppm, which is comparable to those of Ir(III) complex. Notably, the ^{3}PC* plays a key role in conferring oxygen tolerance to the reaction. This occurs because ^{3}PC* can convert molecular oxygen (O_2) into reactive oxygen species (ROS) via either the PET or photoinduced energy transfer (PEnT) process. Subsequently, the generated ROS are

https://doi.org/10.1021/acs.accounts.4c00847
Acc. Chem. Res. 2025, 58, 1581−1595

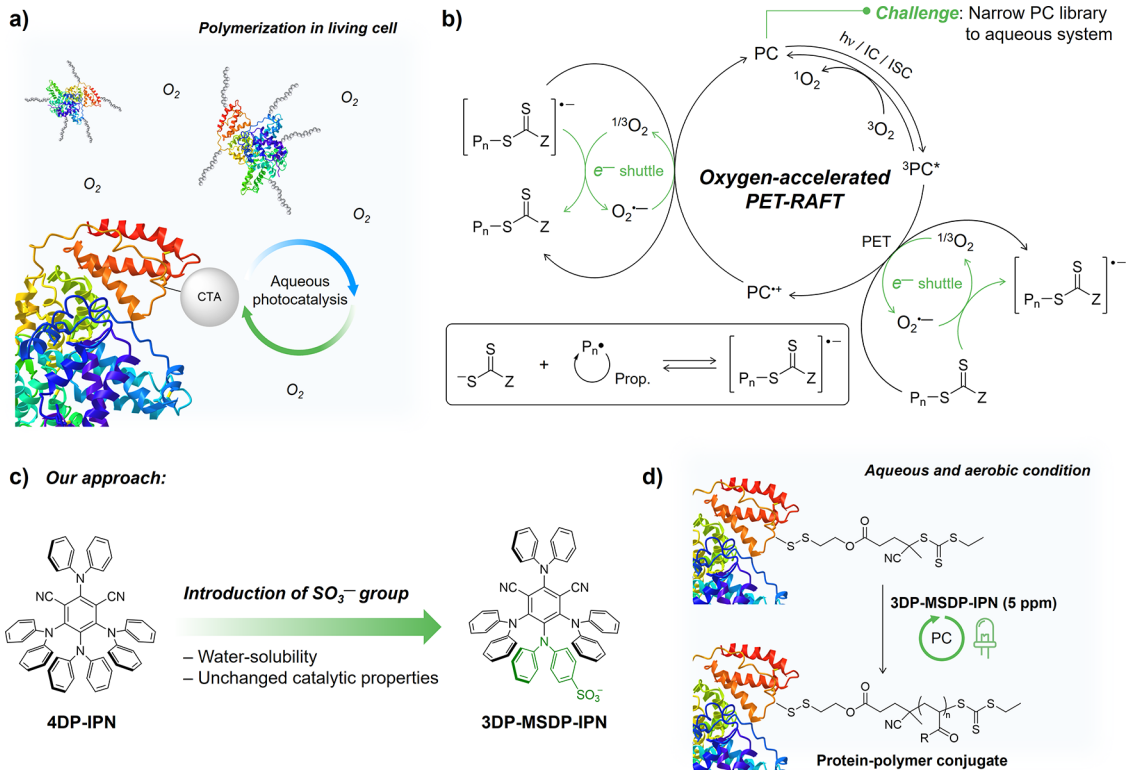

Figure 5. (a) Aqueous PET-RAFT polymerization with high oxygen tolerance. (b) Proposed mechanism of PET-RAFT polymerization accelerated by O_2. (c) PC design strategies for 3DP-MSDP-IPN to enhance water-solubility. (d) Aqueous PET-RAFT polymerization using 3DP-MSDP-IPN under aqueous and aerobic conditions for PPCs.

consumed by DMSO, which is used as a solvent, producing adducts such as dimethyl sulfone and thereby removing O_2 from the reaction medium.

PET-RAFT polymerization has a wide range of applications combining its strong oxygen tolerance,[55,57] with significant potential in bioapplications, particularly for protein−polymer conjugates (PPCs) in living cells. However, applying PET-RAFT to PPCs requires water-soluble PCs, limiting the selection of specific PCs such as Ru(II) complexes, xanthenes, and metalloporphyrins.[55] To address this limitation, we modified 4DP-IPN to enhance its water-solubility by introducing a sulfonate group, which is a water-soluble, biocompatible, and highly stable functional group, into one of the diphenylamine moieties while maintaining its properties (Figure 5).[2] Consequently, we developed 3DP-MSDP-IPN. As anticipated, 3DP-MSDP-IPN (E_{ox}^* = −1.56 V, E_{ox}^0 = 1.02 V, and Φ_F = 0.78; evaluated in DMSO) exhibited similar catalytic properties to those of 4DP-IPN (E_{ox}^* = −1.57 V, E_{ox}^0 = 1.01 V, and Φ_F = 0.85; evaluated in DMSO) while offering improved water-solubility. To verify its feasibility in the PPC application, we conducted PET-RAFT polymerizations of water-soluble acrylates and acrylamides in an aqueous medium using 3DP-MSDP-IPN at 5 ppm under ambient and aerobic conditions. Interestingly, oxygen-acceleration behavior was observed in both organic and aqueous media. This behavior was attributed to the role of superoxide as electron shuttles between ^{3}PC* and chain transfer agents (CTAs), enabling a faster PC cycle (Figure 5b). Subsequently, we successfully demonstrated the synthesis of PPCs by grafting from bovine serum albumin as a model protein, using the water-soluble monomers and 3DP-MSDP-IPN at 50 ppm. Meanwhile, efforts to enhance the water-solubility of cyanoarenes for aqueous photocatalysis have been actively pursued. For example, in 2024, Ouyang et al. reported CO_2 photoreduction in the aqueous medium using 4DP-IPN derivatives functionalized with phosphoric acid.[58] These results, from both our group and Ouyang et al., demonstrate that our PC library can be expanded to aqueous systems utilizing tailored PC modifications.

3. PC DESIGN FOR EFFICIENT PC CYCLE CLOSURE

The design of efficient photoredox catalysis requires a comprehensive understanding of the entire PC cycle, including not only the opening of the PC cycle through the PET process but also the closing of the PC cycle to regenerate the PC. Specifically, the stabilities and reactivities of PC intermediates (i.e., $PC^{\bullet+}$ or $PC^{\bullet-}$) are closely linked to the ability to achieve low PC loadings, which is the key advantage of utilizing ^{3}PC*. Thus, it is essential to design PCs that can efficiently close the PC cycle, tailored to the desired reaction conditions. While the previous sections focused on the opening of PC cycles, this section aims to summarize our studies that emphasize the importance of closing the PC cycle, highlighting the intricate processes involved in PC regeneration and their impact on the overall catalytic efficiency.

3.1. ATRP with Photoredox/Copper Dual Catalysis

ATRP with photoredox/copper dual catalysis, combining the merits of both photoinduced ATRP and photoredox-mediated ATRP, has been recently proposed by Yagci,[59] Strehmel,[60] and Matyjaszewski.[61] This approach has gained prominence as a solution to an inefficient deactivation—entropically unfavorable transition from three-body-species to two-body-species—in photoredox-mediated ATRP. This method utilizes Cu(II)-Br_2/L (L = ligand) as a deactivator to control the ATRP

https://doi.org/10.1021/acs.accounts.4c00847
Acc. Chem. Res. 2025, 58, 1581−1595

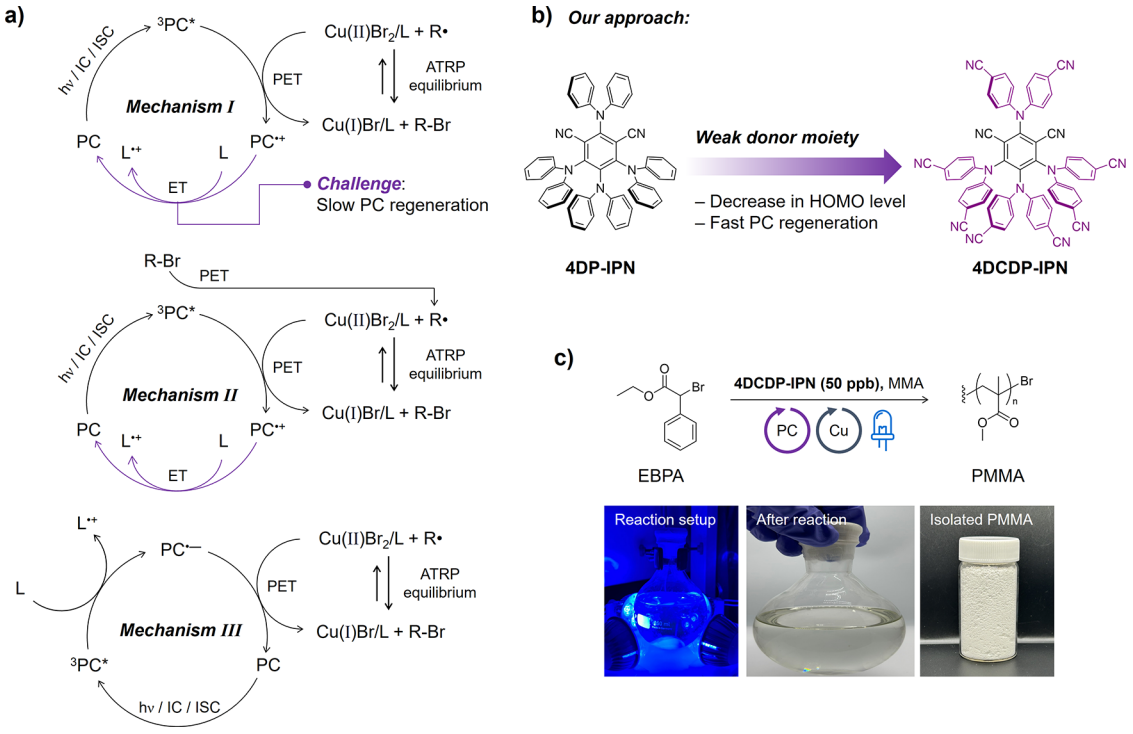

Figure 6. (a) Proposed mechanisms of ATRP with photoredox/copper dual catalysis. (b) PC design strategies for 4DCDP-IPN to enhance its regeneration ability. (c) Oxygen-tolerant large-scale ATRP with photoredox/copper dual catalysis using 4DCDP-IPN at 50 ppb without any degassing process. Images of the reaction batch and isolated products are also provided.

equilibrium, suppressing irreversible radical termination and enabling the production of well-controlled polymers.[62] However, despite the advancement in ATRP with photoredox/copper dual catalysis, the selection of PCs still relied on the inefficient and unbiased screening of PC scaffolds that have been effective in other RDRP methods. Moreover, PC loadings remained relatively high, typically ranging from 10 to 1000 ppm, due to a still unclear mechanistic understanding of the initiation mechanism and PC regeneration.

We addressed the high PC loading in ATRP with photoredox/copper dual catalysis through a PC design strategy based on detailed mechanistic studies. Currently, three mechanisms for ATRP with photoredox/copper dual catalysis have been proposed (Figure 6a). In our investigations on these mechanisms, we noticed that most of our PC library can easily reduce Cu(II)Br_2/L (E_{red}^0 = −0.11 to −0.30 V) with highly fast k_{PET} close to the diffusion limit. Based on the rapid PET to Cu(II)Br_2/L, we tailored the PC design strategy to *Mechanism I*,[3] which is primarily focusing on a PC regeneration process rather than relying on the PET process to directly activate dormant species, as seen in *Mechanism II*. For the favorable PC regeneration, the PC must have a more positive E_{ox}^0 than that of the employed ligand. To achieve this, we introduced a strong electron-withdrawing group (−CN group) into the donor moieties of 4DP-IPN to lower the highest occupied molecular orbital (HOMO) energy making E_{ox}^0 of a tailored PC more positive than that of 4DP-IPN (E_{ox}^0 = 1.01 V) (Figure 6b). This resulted in the discovery of 4DCDP-IPN, which exhibits a significantly higher E_{ox}^0 of 1.66 V compared to the ligand, tris(2-pyridylmethyl)amine (TPMA) (E_{ox}^0 = 0.99 V), thereby facilitating the PC regeneration. In addition, 4DCDP-IPN exhibits a long T_1 state lifetime ($\tau_{delayed.} \approx 196$ μs), which increases the ^{3}PC* concentration, accelerating the ET process to Cu(II)Br_2/L and compensating for the less negative E_{ox}* of 4DCDP-IPN (E_{ox}* = −0.75 V). Based on its catalytic properties, we successfully synthesized PMMA with an ultralow PC loading of only 50 parts per billion (ppb) accompanied by high PC stability, and demonstrated large-scale reactions without needs for oxygen removal[63] (Figure 6c). These investigations validate the importance of the mechanism-driven PC design strategy to address challenges in the organic transformations.

3.2. Photocatalytic Reductive Dehalogenation

To elucidate the PC intermediates in photocatalysis, we investigated a photocatalytic reductive dehalogenation of aryl bromides/chlorides bearing electron-donating groups; these substrates have been considered highly challenging to activate. Typically, the dehalogenation of these substrates proceeds via the reductive quenching cycle, with the $PC^{\bullet-}$ generated in this process believed to play a crucial role. Notably, König et al. reported that the reductive dehalogenation of aryl chlorides occurs through a consecutive PET (ConPET) mechanism wherein $PC^{\bullet-}$ is photoexcited to become highly reducing $PC^{\bullet-}$* by a multiphoton process.[64] Similarly, Wickens et al. successfully demonstrated the reductive dehalogenation of aryl chlorides utilizing the photoexcited $PC^{\bullet-}$ of 4DP-IPN, generated via an electrophotocatalytic method.[65]

Our initial focus was on 4DP-IPN to assess the photochemical generation of its radical anion under typical photocatalytic dehalogenation conditions (Figure 7a).[4] Under visible light irradiation and the presence of *N,N*-diisopropylethylamine (DIPEA) as a sacrificial reductant, we observed the generation of 4DP-IPN$^{\bullet-}$ with red-shifted UV−visible absorption; it exhibited a sufficiently long lifetime to be observed with the naked eye. Interestingly, after the reaction solutions were fully exposed to air to quench the 4DP-IPN$^{\bullet-}$, we observed that its UV−visible absorption spectra did not

https://doi.org/10.1021/acs.accounts.4c00847
Acc. Chem. Res. 2025, 58, 1581−1595

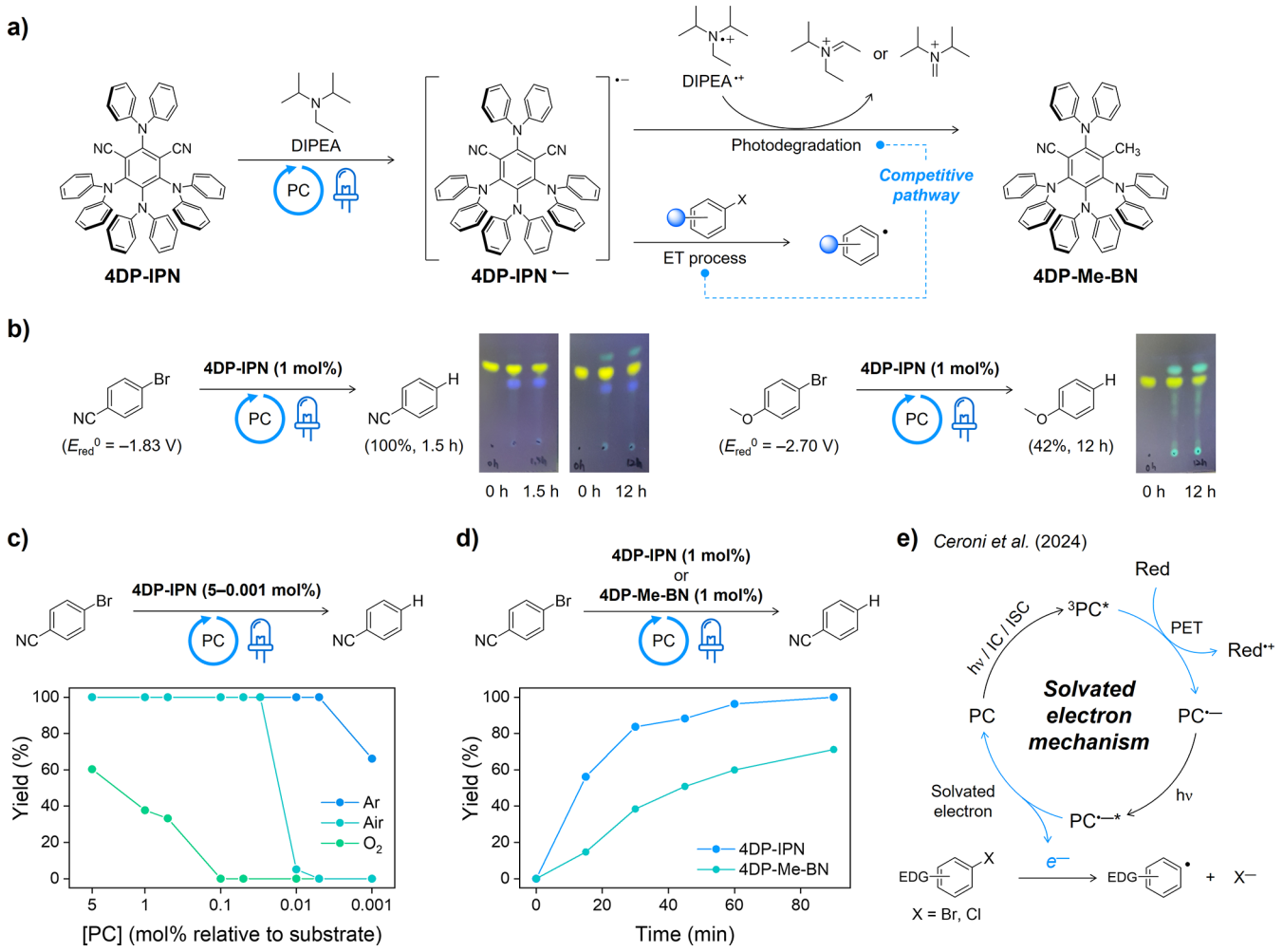

Figure 7. (a) Competitive interaction between PC degradation and the ET process. (b) Monitored PC degradation during the reductive dehalogenation. (c) Highly efficient photoredox reductive dehalogenation using 4DP-IPN. (d) Comparison of reaction kinetics with 4DP-IPN and 4DP-Me-BN in the reductive dehalogenation. (e) Mechanism of solvated electron process by Ceroni et al.[67]

fully recover to 100% of the neutral PC's, indicating that some of the 4DP-IPN had degraded. To confirm the degradation, we monitored the reaction solution with thin-layer chromatography (TLC) and noted the generation of blue-shifted emitting compounds. After these new emitting compounds were isolated, we confirmed that the PC adduct (i.e., 4DP-Me-BN) was mainly substituted by an alkyl group likely generated from the β-scission of the oxidized DIPEA ($DIPEA^{\bullet+}$)[66] at the position of the −CN groups in the acceptor moiety (Figure 7a). This substitution leads to a significant increase in the LUMO energy (e.g., for 4DP-IPN/4DP-Me-BN, from −2.60 eV to −2.17 eV) compared to the rise in the HOMO energy (e.g., for 4DP-IPN/4DP-Me-BN, from −5.63 eV to −5.52 eV), thereby altering electrochemical and photophysical properties and enabling more negative E_{red}^0 and less visible-light absorption.

To further investigate the formation of $PC^{\bullet-}$, we assessed nine additional cyanoarenes, substituted with various donor moieties. After their radical anions were photochemically generated under the same conditions with 4DP-IPN, some trends were revealed: for the efficient formation of $PC^{\bullet-}$, the cyanoarene PCs should have (i) appropriate E_{red}^* to involve PET with DIPEA and (ii) the ability to generate long-lived T_1 states both to accelerate PET and to slow down BET process with the $DIPEA^{\bullet+}$. Furthermore, we investigated their PC degradations and observed that the degradation of cyanoarenes, involving efficient $PC^{\bullet-}$ generation, typically occurred. This indicates that high $PC^{\bullet-}$ concentration can promote PC degradation. After the isolation of the degraded PCs, they were found to be mainly substituted by the alkyl group at the −CN groups in the acceptor moiety. However, when labile groups (i.e., −CN or F) were present in the donor moieties, the PC degradation results in unidentified and complex mixtures of PC adducts.[4]

Subsequently, we investigated the PC degradation behavior in actual photoreactions, monitoring the PC degradation during a reductive dehalogenation of 4-bromobenzonitrile (E_{red}^0 = −1.83 V) and 4-bromoanisole (E_{red}^0 = −2.70 V) using 4DP-IPN (E_{red}^0 = −1.66 V) as PC. In the dehalogenation of 4-bromobenzonitrile, degradation of 4DP-IPN was not observed until the total conversion of 4-bromobenzonitrile. However, after the completion of the reaction, the generation of 4DP-Me-BN was observed in the TLC results (Figure 7b). Leveraging this high stability of 4DP-IPN until the reaction is complete, we additionally demonstrated that an exceptionally low PC loading of 0.005 mol % relative to 4-bromobenzonitrile while maintaining the oxygen tolerance (Figure 7c).[4] Conversely, in the dehalogenation of 4-

https://doi.org/10.1021/acs.accounts.4c00847
Acc. Chem. Res. 2025, 58, 1581−1595

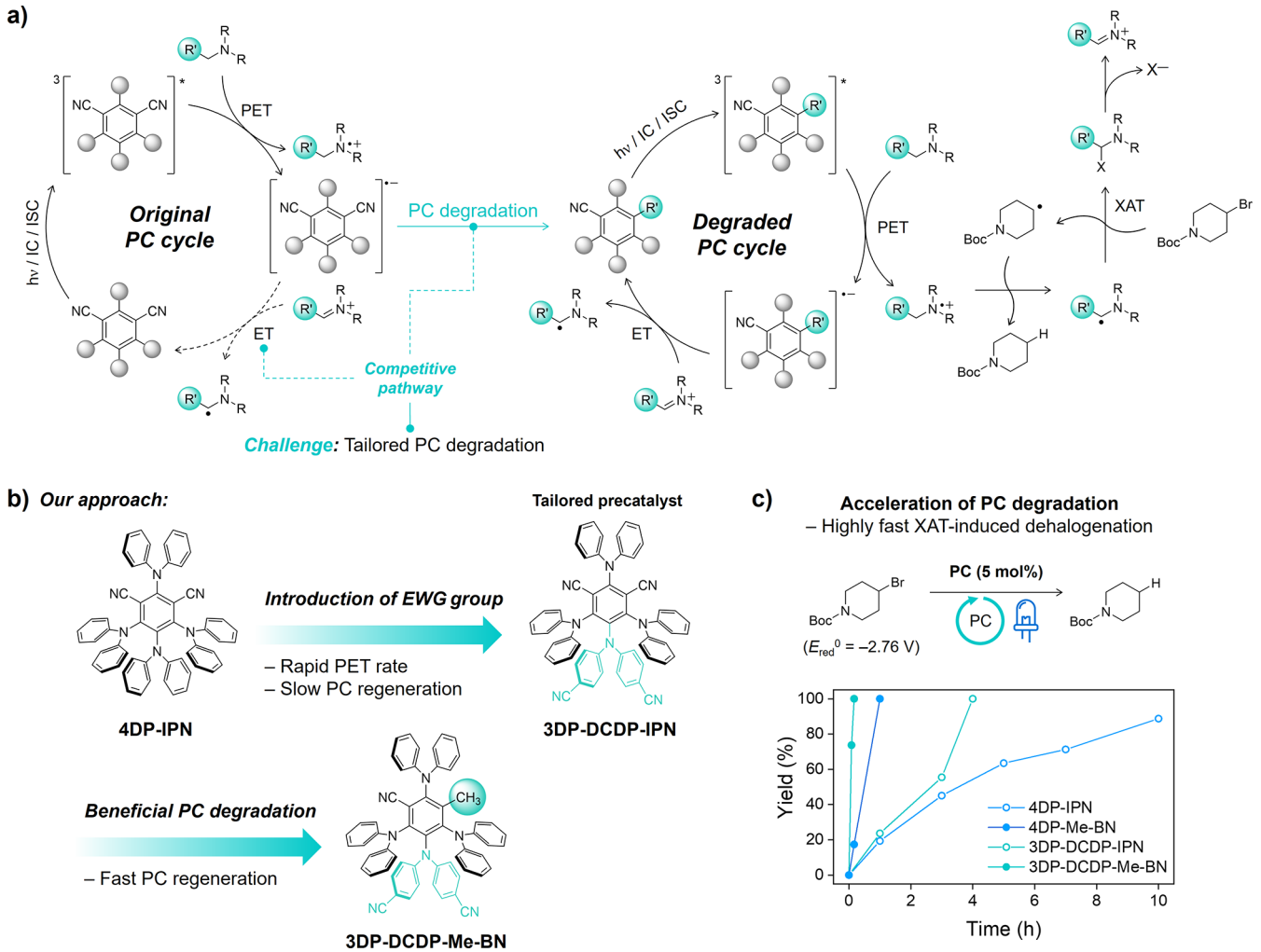

Figure 8. (a) Proposed mechanism of XAT-induced dehalogenation leveraging beneficial PC degradation. (b) PC design strategies for tailoring 3DP-DCDP-IPN as the precatalyst to accelerate PC degradation. (c) Comparison of reaction kinetics with 4DP-IPN, 4DP-Me-BN, 3DP-DCDP-IPN, and 3DP-DCDP-Me-BN in the XAT-induced dehalogenation.

bromoanisole, the generation of 4DP-Me-BN was observed from the initial stage of the reaction. This indicates that the PC degradation pathway competes with the ET process between $PC^{\bullet-}$ and the target substrate, thereby governing the concentration of $PC^{\bullet-}$ (Figure 7a). Additionally, we compared the original PC and degraded PC in the reductive dehalogenations of 4-bromobenzonitrile (Figure 7d) and 4-bromoanisole by using 4DP-IPN ($E_{red}^0 = -1.66$ V, $E_{red}^* = 0.63$ V, and $\tau_{delayed.} \approx 122$ μs)[68] and 4DP-Me-BN ($E_{red}^0 = -2.05$ V, $E_{red}^* = 0.54$ V, and $\tau_{delayed.} \approx 407$ μs) as PCs.[68] Under the same conditions, 4DP-Me-BN typically resulted in lower yields than 4DP-IPN. Considering that 4DP-Me-BN has more negative E_{red}^0 and decent long-lived T_1 generation, we infer that its lower performance is attributable to the low visible-light absorption of 4DP-Me-BN and its less positive E_{red}^*.

Notably, by using 4DP-IPN as PC, we achieved the reductive dehalogenation of 4-bromoanisole and 4-chloroanisole ($E_{red}^0 = -2.80$ V)—substrates whose activation has been considered highly challenging—with 38% and 74% yields within 48 h, respectively.[4] This outcome could not be explained solely by the redox potentials of 4DP-IPN and these substrates. Therefore, we posit that the reaction might proceed through the ConPET mechanism and/or via the halogen-atom-transfer (XAT) process.[69] However, Ceroni et al. recently revealed that, solvated electrons generated by the photoexcitation of $4DP\text{-}IPN^{\bullet-}$ confer the exceptional reducing power rather than the direct transfer of electron by $4DP\text{-}IPN^{\bullet-}$ to the aryl halides because of the extremely short excited-state lifetime of $4DP\text{-}IPN^{\bullet-*}$ ($\tau \approx 20$ ps) (Figure 7e).[67]

3.3. Photocatalytic XAT-Induced Dehalogenation

The aforedescribed results motivated us to explore the impact of the degradation of cyanoarenes on the overall efficiency of photocatalytic reactions. Therefore, we investigated whether this degradation occurs in other dehalogenation processes, such as XAT-induced dehalogenation. In this process, α-amino radicals, generated from the oxidized amines, abstract a halide atom to cleave the C–X bond.[69] Initially, we performed the XAT-induced dehalogenation of 4-bromo-(*N*-Boc)-piperidine ($E_{red}^0 = -2.76$ V) to examine the PC degradation behaviors by using 4Cz-IPN, a cyanoarene substituted with carbazole, as PC, as reported by Leonori et al.,[69] who utilized thiyl radical as an oxidant for PC regeneration. We observed a 15% conversion of 4-bromo-(*N*-Boc)-piperidine within 7 h in the presence of thiol; in contrast, under conditions without thiol, a 100% conversion was achieved within 12 h. Interestingly, in the absence of thiol, rapid degradation of 4Cz-IPN was observed within 0.5 h; following the isolation of PC adducts,

https://doi.org/10.1021/acs.accounts.4c00847
Acc. Chem. Res. 2025, 58, 1581–1595

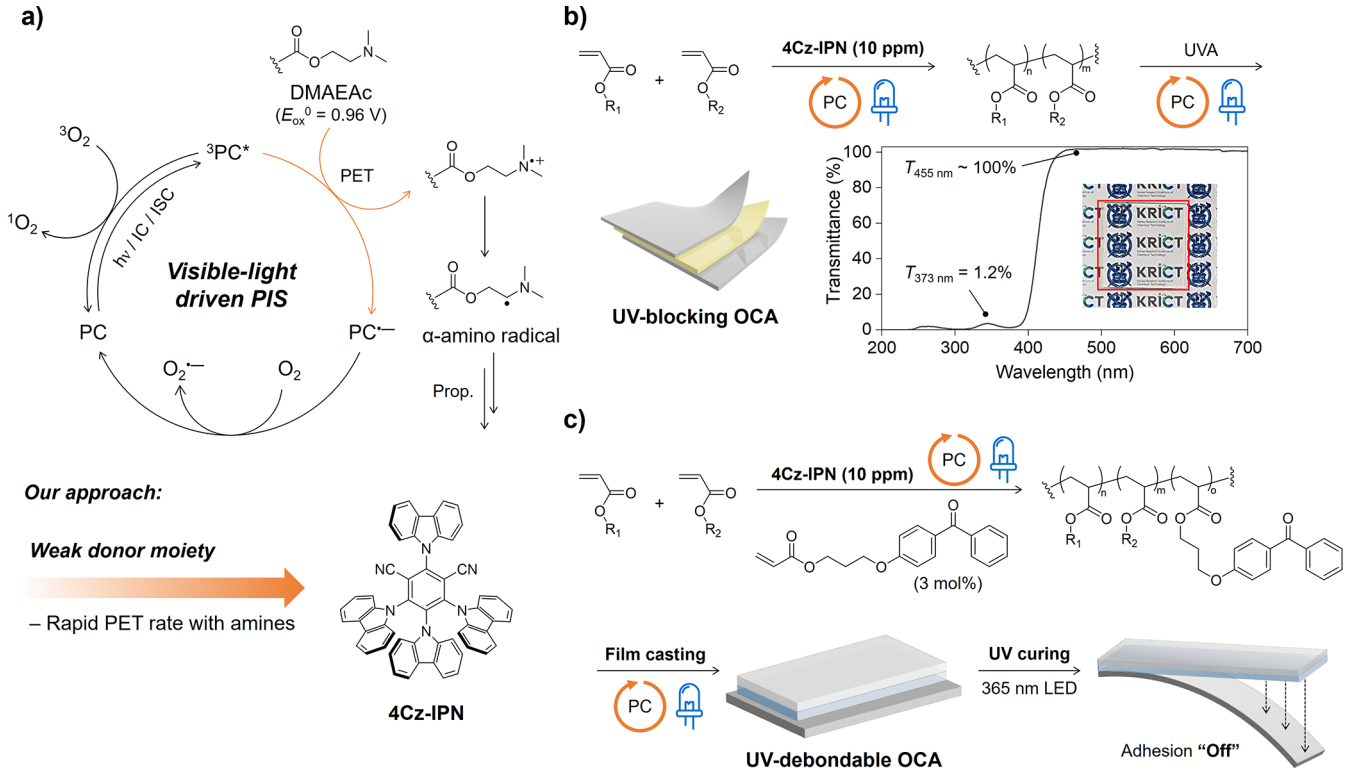

Figure 9. (a) Proposed mechanism of PIS using 4Cz-IPN and amine-based co-initiator. (b) Synthesis of UV-blocking OCAs under ambient conditions using 4Cz-IPN and amines, incorporating UVA as a functionalizing agent. (c) Synthesis of UV-debondable OCAs under ambient conditions using 4Cz-IPN and amine-based co-initiator, incorporating a benzophenone-based acrylate as a functionalizing monomer.

we characterized them as a mixture of 4Cz-R-BN (R = Me or Et), which is alkylated at the position of the −CN group in the acceptor moiety.[4] On this basis, we hypothesized that PC degradation in XAT-induced dehalogenation potentially enhances overall reactivity. PC degradation increases the LUMO energy level, thereby making its E_{red}^0 more negative, promoting ET with somewhat electron acceptors. Consequently, the PC cycle is accelerated, resulting in high concentrations of α-amino radicals (Figure 8a). Based on this insight, we envisioned the introduction of the concept of beneficial PC degradation and designed its precatalyst to enhance the reactivity of XAT-induced dehalogenation.

To identify the catalytic properties that promote PC degradation, we first compared the degradation rates of 4Cz-IPN (E_{red}^0 = −1.2 1 V) and 4DP-IPN (E_{red}^0 = −1.66 V) in thiol-free conditions by using DIPEA as the sacrificial reductant in XAT-induced dehalogenation with 4-bromo-(*N*-Boc)-piperidine as the model substrate. We observed that 4Cz-IPN was completely degraded within 0.5 h, whereas a significant portion of 4DP-IPN remained intact even after the reaction was complete (10 h). This suggests the presence of the species oxidizing the 4DP-IPN$^{\bullet-}$ and we attributed this electron acceptor to iminium ions ($E_{red}^0 \approx -1.55$ V) in the reaction mixtures. Subsequently, to confirm our hypothesis that the PC degradation would be beneficial to the XAT-induced dehalogenation, we performed comparative analyses using other cyanoarenes, 4DP-IPN (E_{red}^0 = −1.66 V) and 4DP-Me-BN (E_{red}^0 = −2.05 V), in the XAT-induced dehalogenation of 4-bromo-(*N*-Boc)-piperidines. As hypothesized, the use of 4DP-IPN afforded 89% yield after 10 h, whereas 4DP-Me-BN showed a 100% yield within 1 h (Figure 8c). Accordingly, we set the criteria to design the precatalyst that efficiently undergoes the PC degradation to enhance the reactivity of XAT-induced dehalogenation. The precatalyst should satisfy the following conditions: (i) the PC$^{\bullet-}$ must be efficiently generated; (ii) this generated PC$^{\bullet-}$ should be alkylated at the position of the −CN group; and (iii) the rate at which PC$^{\bullet-}$ is alkylated into its degraded form must be faster than that at which it regenerates to the neutral PC.

To realize this design, we modified 4DP-IPN by introducing an electron-withdrawing −CN group into one of diphenyl amines to precisely decrease the HOMO energy for the tailored precatalyst, 3DP-DCDP-IPN (E_{red}^0 = −1.51 V, E_{red}^* = 0.92 V, and $\tau_{delayed.} \approx 59\ \mu s$) (Figure 8b). To examine whether 3DP-DCDP-IPN is efficiently one-electron reduced, we compared 4DP-IPN and 3DP-DCDP-IPN in the rate constant of PET with DIPEA. As anticipated, 3DP-DCDP-IPN (k_{PET} = 2.9 × 10^7 M^{-1} s^{-1}) was found to have faster PET rate constants than 4DP-IPN (k_{PET} = 4.8 × 10^5 M^{-1} s^{-1}). Furthermore, to characterize its degraded form, 3DP-DCDP-Me-BN (E_{red}^0 = −1.94 V, E_{red}^* = 0.67 V, and $\tau_{delayed.} \approx 497\ \mu s$), we prepared 3DP-DCDP-Me-BN following a previously reported procedure.[4] Subsequently, by monitoring the reaction mixture of XAT-induced dehalogenation with 4-bromo-(*N*-Boc)-piperidine via TLC, we confirmed that the degradation of 3DP-DCDP-IPN to its alkylated form occurred within 1 h. We examined performance of 3DP-DCDP-Me-BN as PC in XAT-induced dehalogenation, exhibiting 100% yield within 10 min. Finally, by using 3DP-DCDP-IPN as precatalyst, we successfully activated 4-bromo-(*N*-Boc)-piperidine in a significantly shorter time, compared to not only other uses of 4DP-IPN but also those previously reported by Leonori et al. (Figure 8c).[69] This result is attributable to the highly reducing E_{red}^0 value, suitable visible-light absorption, and extended T_1

https://doi.org/10.1021/acs.accounts.4c00847
Acc. Chem. Res. 2025, 58, 1581−1595

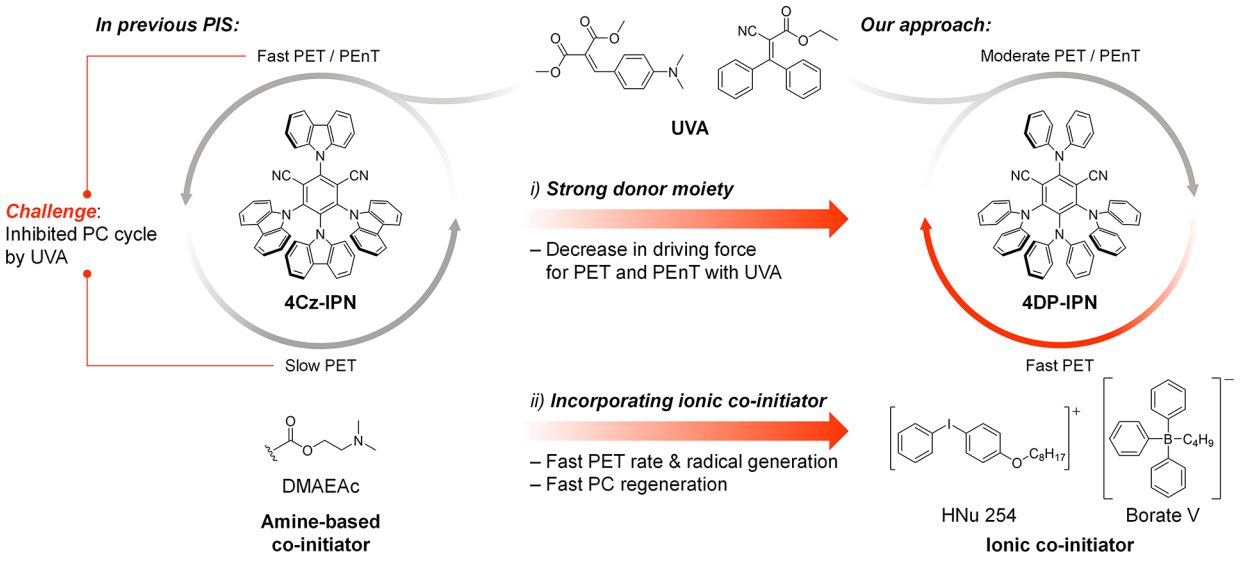

Figure 10. Inhibition of the PC cycle of 4Cz-IPN in the presence of UVA and advanced PIS design strategies to overcome this inhibition, including the use of 4DP-IPN as the PC and incorporation of ionic co-initiators.

state lifetime. Our investigations potentially contribute not only to organic reactions[18,70]—wherein $PC^{\bullet-}$ serves as the core intermediate—encouraging chemists to consider potential PC degradation,[71] but also to better design PC strategies that tailor precatalysts for harnessing their degraded forms.

4. FREE RADICAL POLYMERIZATION

Photoredox catalysis has been employed not only in RDRP but also in the free radical polymerization, with organic dye-sensitized photoinitiating systems (PISs) being a notable example. Over the past decade, PISs have advanced significantly, particularly through the pioneering works of Fouassier and Lalevée.[72−74] More recently, Page at al. actively reported rapid visible-light-driven PISs applicable in 3D printing using BODIPY-based PCs.[75,76] These PISs have been widely applied in various fields, including 3D/4D printing materials,[77] dental resins,[78] and adhesives.[73]

However, visible-light-driven PISs face challenges related to a coloration from PC residue in the produced resins, which limits their optical applications. To address this issue, we employed cyanoarene-based PCs to significantly lower the overall PC loading.[33] Our strategy involved utilizing the reductive quenching cycle with cyanoarenes and amines (Figure 9a), which enabled reduced PC loading due to the high effective concentration of $^3PC^*$. This approach eliminated the need for additional radical precursors, as α-amino radicals, generated from the amine-based co-initiators, acted as initiating species.[66] The system also exhibited a high degree of oxygen tolerance, which was attributed to the accelerated closure of the PC cycle by $O_2^{\bullet-}$ and/or additional generation of α-amino radicals from peroxy radicals (i.e., ROO•). After screening various cyanoarenes and amines, we identified a combination, consisting of 4Cz-IPN (E_{red}^* = 1.47 V),[33] and 2-(dimethylamino) ethyl acetate (DMAEAc) as the most effective, exhibiting the fastest polymerization kinetics. However, this result was counterintuitive, as DMAEAc has a higher E_{ox}^0 of 0.96 V than other amines (e.g., DIPEA, E_{ox}^0 = 0.62 V),[33] resulting in an approximately 10−100 times slower PET rate constant utilizing 4Cz-IPN. To investigate this discrepancy, we performed density functional theory calculations, which revealed that DMAEAc possessed a lower activation energy for α-amino radical formation from its oxidized form compared with those of other amines (e.g., DIPEA).[33] This finding indicated that the rate-determining step of the initiation process was not the PET process but rather the formation of α-amino radicals. Under optimized PIS conditions, we demonstrated visible-light-driven PISs without an oxygen removal process, achieving the synthesis of highly visible-light-transparent acrylic optically clear adhesives (OCAs) (Figure 9b and 9c).

Using this visible-light-driven PIS, we demonstrated two types of OCAs. The first is UV-blocking OCA containing UV-absorbers (UVAs) (Figure 9b).[33] Due to the high UV absorbance of UVA, conventional UV-photocuring methods, that rely on UV-photoinitiators, are hindered. As expected, we observed that UV-blocking OCA was cured significantly faster with our PIS than with conventional UV-photocuring methods. Consequently, our PIS enabled the development of OCA with high transmittance in the visible-light region while maintaining strong absorbance in the UV region. The second application is UV-debondable OCA, which utilizes the orthogonality of selective activation of different types of reactions under irradiation at specific wavelengths (Figure 9c). We developed functionalized OCA by incorporating UV-responsive benzophenone-derived acrylates, which undergo Norrish Type II reactions to form covalent bonds within the polymer network.[34] Following visible-light curing, the OCA is postcured under UV irradiation, activating the UV-responsive acrylates to enhance cohesive properties, ultimately facilitating delamination between the OCA and substrate. Furthermore, we applied this UV-debondable OCA to actual display-manufacturing processes, using ultra-thin glass (UTG) as the substrate. The results showed that UTG could be easily separated and recycled without any adhesive residue, highlighting the potential applicability of this approach in sustainable plastics, electronics, and display technologies.

Meanwhile, the synthesis of UV-blocking OCA was considerably slowed down in the presence of UVA. Through mechanistic studies and characterization of UVAs, we discovered that fast ET and/or EnT processes between UVA

https://doi.org/10.1021/acs.accounts.4c00847
Acc. Chem. Res. 2025, 58, 1581−1595

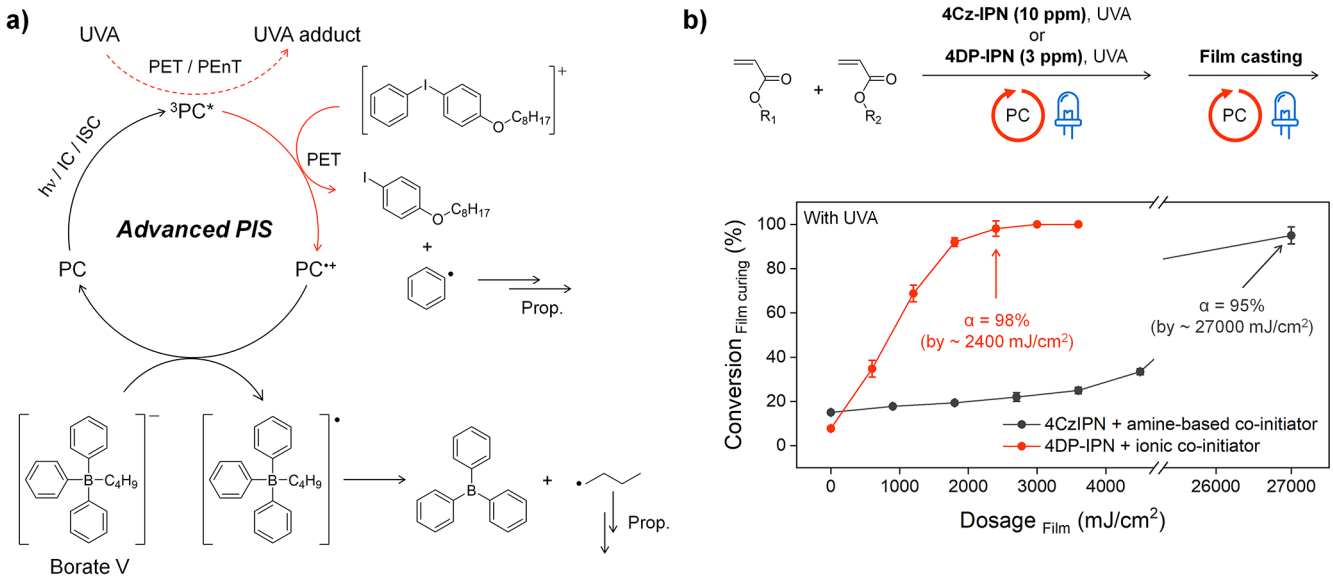

Figure 11. (a) Proposed mechanism of PIS using 4DP-IPN and ionic co-initiators. (b) Rapid and efficient PIS for synthesizing UV-blocking OCA using 4DP-IPN and ionic co-initiators.

and photoexcited 4Cz-IPN led to a decrease in the concentration of ^{3}PC*, thus inhibiting the PET process between 4Cz-IPN with DMAEAc (Figure 10). To overcome this inhibition, we employed two strategies: (i) the use of a PC with a higher HOMO energy to lower the energy of T_1 state, suppressing the quenching of ^{3}PC* by UVA, and (ii) the utilization of ionic co-initiators to accelerate the PC cycle and enable rapid radical generation. We initially replaced 4Cz-IPN with 4DP-IPN, which not only incorporated electron-donating groups, but also efficiently generated long-lived T_1 states. In addition, inspired by Page et al.,[77] instead of the amine-based co-initiator, we utilized iodonium and borate derivatives as co-initiators (i.e., HNu 254 and Borate V). In the Stern−Volmer plot for 4DP-IPN and the components in the new PIS, we observed, as expected, that 4DP-IPN exhibited approximately 10 times faster ET rate constants with the ionic co-initiators compared with the quenching rate constants by UVA. This suggested that the PET with the ionic co-initiators is less inhibited by UVA. Consequently, by utilizing our new PIS, we successfully demonstrated the highly rapid curing of UV-blocking OCA, requiring 10 times less light dosage (2400 mJ/cm^2) compared with that needed when using 4Cz-IPN and amines (27000 mJ/cm^2) (Figure 11).

5. CONCLUSION

This *Account* summarized our contributions to visible-light-driven organic transformations utilizing PCs in the T_1 state. The role of ^{3}PC* in the polymerization process was crucial, as it increased the effective concentration of the PC in the medium, enhanced its reactivity with target substrates, and reduced BET process, ultimately increasing the overall photocatalytic efficiency. Utilizing our strongly twisted donor−acceptor structured PC design platform, we adopted a mechanism-driven strategy to identify efficient PCs with the desired catalytic properties for specific reactions. Furthermore, we established the following criteria for designing PCs for efficient visible-light-driven polymerizations: (i) efficient T_1 state generation, (ii) appropriate redox potentials and excited-state energies, and (iii) the ability to be rapidly regenerated. Subsequently, using the discovered PCs, we were able to successfully synthesize eco-friendly and economically viable polymers for a broad range of applications, including controlled polymerizations, biomedical reactions and adhesives. Our systematic approach not only highlighted the potential of T_1 states in the polymerizations but also set a framework for future PC development in this field. This framework emphasized the need for a deeper mechanistic understanding to select PC and consequently to drive innovation and efficiency in the polymerizations. As efforts have been made to shift the energy used in photocatalytic reactions from UV light to visible light, we anticipate the emergence of new PC libraries and novel polymerization methodologies that would enable further advancements beyond the current photochemical processes.

AUTHOR INFORMATION

Corresponding Authors

Johannes Gierschner − *Madrid Institute for Advanced Studies, IMDEA Nanociencia, 28049 Madrid, Spain;* orcid.org/0000-0001-8177-7919; Email: johannes.gierschner@imdea.org

Min Sang Kwon − *Department of Materials Science and Engineering, Research Institute of Advanced Materials, Seoul National University, Seoul 08826, Republic of Korea;* orcid.org/0000-0002-1485-7588; Email: minsang@snu.ac.kr

Authors

Yonghwan Kwon − *Department of Materials Science and Engineering, Research Institute of Advanced Materials, Seoul National University, Seoul 08826, Republic of Korea;* orcid.org/0000-0003-1459-8149

Woojin Jeon − *Department of Materials Science and Engineering, Research Institute of Advanced Materials, Seoul National University, Seoul 08826, Republic of Korea*

Complete contact information is available at: https://pubs.acs.org/10.1021/acs.accounts.4c00847

https://doi.org/10.1021/acs.accounts.4c00847
Acc. Chem. Res. 2025, 58, 1581−1595

Notes

The authors declare no competing financial interest.

Biographies

Yonghwan Kwon received his B.S. degree in Chemistry from Ulsan National Institute of Science & Technology (UNIST) in 2018. Then, he pursued his Ph.D. in Material Science and Engineering (MSE) at UNIST under the guidance of Prof. Min Sang Kwon. After earning his Ph.D., he continued his research career as a postdoctoral fellow at Seoul National University (SNU) with Prof. Min Sang Kwon in 2023. His research interests span polymer chemistry, organic chemistry, and photochemistry.

Woojin Jeon received his B.S. degree in Polymer Science and Engineering from Pusan National University in 2023. Since 2023, he has been pursuing his Ph.D. in MSE at SNU under the supervision of Prof. Min Sang Kwon. His research interests include organic chemistry, photochemistry, and polymer chemistry.

Johannes Gierschner received his Ph.D. in Physical Chemistry from the University of Tübingen (UT) in 2000. He has held research positions at UT, the University of Mons (UM), and Georgia Tech in Atlanta. In 2008, he joined IMDEA Nanoscience as a Senior Research Professor and was a Ramón y Cajal fellow from 2008 to 2013. In 2014, he habilitated at UT and has held an Adjunct Professor position there since then. He is a regular visiting researcher at the University of Valencia (since 2014) and at SNU (since 2008) and held Visiting Professor positions at SNU and UM in 2014 and 2015. His research integrates optical spectroscopy and computational chemistry to elucidate structure−property and −process relationships in conjugated organic materials for optoelectronics, energy conversion, and materials science.

Min Sang Kwon received his B.S. degrees in Chemistry and MSE from SNU. He earned his Ph.D. in Chemistry at SNU under the supervision of Prof. Eun Lee. After completing his postdoctoral studies at SNU with Prof. Soo Young Park, he moved to the University of Michigan to work with Prof. Jinsang Kim. In 2016, he began his independent academic career at UNIST as an Assistant Professor. In 2020, he returned to his alma mater, SNU, where he is currently an Associate Professor in MSE. He is a member of the Young Korean Academy of Science and Technology and serves on the editorial board of the *Journal of Polymer Science*. His research interests include organic chemistry, photochemistry, and polymer chemistry.

■ ACKNOWLEDGMENTS

We are grateful to past and present co-workers for their invaluable contributions to the insight in the photophysics described in this Account from the group of Prof. J. Gierschner and Prof. R. Wannemacher at IMDEA Nanoscience. We also thank affectionate supports from Prof. Hyun-Joong Kim at SNU. This work was supported by the National Research Foundation of Korea (NRF) grant funded by the Korea government (MSIT) (No. 2021R1A5A1030054), by the Spanish Ministerio de Ciencia e Innovación (MICIN-FEDER) project (PID2022-138222NB-C21), and the Severo Ochoa program for Centers of Excellence in R&D of the MICIN (CEX2020-001039-S).

■ REFERENCES

(1) Singh, V. K.; Yu, C.; Badgujar, S.; Kim, Y.; Kwon, Y.; Kim, D.; Lee, J.; Akhter, T.; Thangavel, G.; Park, L. S.; Lee, J.; Nandajan, P. C.; Wannemacher, R.; Milián-Medina, B.; Lüer, L.; Kim, K. S.; Gierschner, J.; Kwon, M. S. Highly Efficient Organic Photocatalysts Discovered via a Computer-Aided-Design Strategy for Visible-Light-Driven Atom Transfer Radical Polymerization. *Nat. Catal.* **2018**, *1*, 794−804.

(2) Lee, Y.; Kwon, Y.; Kim, Y.; Yu, C.; Feng, S.; Park, J.; Doh, J.; Wannemacher, R.; Koo, B.; Gierschner, J.; Kwon, M. S. A Water-Soluble Organic Photocatalyst Discovered for Highly Efficient Additive-Free Visible-Light-Driven Grafting of Polymers from Proteins at Ambient and Aqueous Environments. *Adv. Mater.* **2022**, *34*, 2108446.

(3) Jeon, W.; Kwon, Y.; Kwon, M. S. Highly Efficient Dual Photoredox/Copper Catalyzed Atom Transfer Radical Polymerization Achieved through Mechanism-Driven Photocatalyst Design. *Nat. Commun.* **2024**, *15*, 5160.

(4) Kwon, Y.; Lee, J.; Noh, Y.; Kim, D.; Lee, Y.; Yu, C.; Roldao, J. C.; Feng, S.; Gierschner, J.; Wannemacher, R.; Kwon, M. S. Formation and Degradation of Strongly Reducing Cyanoarene-Based Radical Anions towards Efficient Radical Anion-Mediated Photoredox Catalysis. *Nat. Commun.* **2023**, *14*, 92.

(5) Kwon, Y.; Lee, S.; Kim, J.; Jun, J.; Jeon, W.; Park, Y.; Kim, H. J.; Gierschner, J.; Lee, J.; Kim, Y.; Kwon, M. S. Ultraviolet Light Blocking Optically Clear Adhesives for Foldable Displays via Highly Efficient Visible-Light Curing. *Nat. Commun.* **2024**, *15*, 2829.

(6) Yoon, T. P.; Ischay, M. A.; Du, J. Visible Light Photocatalysis as a Greener Approach to Photochemical Synthesis. *Nat. Chem.* **2010**, *2*, 527−532.

(7) Narayanam, J. M. R.; Stephenson, C. R. J. Visible Light Photoredox Catalysis: Applications in Organic Synthesis. *Chem. Soc. Rev.* **2011**, *40*, 102−113.

(8) Nicewicz, D. A.; MacMillan, D. W. C. Merging Photoredox Catalysis with Organocatalysis: The Direct Asymmetric Alkylation of Aldehydes. *Science* **2008**, *322*, 77−80.

(9) Ischay, M. A.; Anzovino, M. E.; Du, J.; Yoon, T. P. Efficient Visible Light Photocatalysis of [2 + 2] Enone Cycloadditions. *J. Am. Chem. Soc.* **2008**, *130*, 12886−12887.

(10) Narayanam, J. M. R.; Tucker, J. W.; Stephenson, C. R. J. Electron-Transfer Photoredox Catalysis: Development of a Tin-Free Reductive Dehalogenation Reaction. *J. Am. Chem. Soc.* **2009**, *131*, 8756−8757.

(11) Zeitler, K. Photoredox Catalysis with Visible Light. *Angew. Chem., Int. Ed.* **2009**, *48*, 9785−9789.

(12) Prier, C. K.; Rankic, D. A.; MacMillan, D. W. C. Visible Light Photoredox Catalysis with Transition Metal Complexes: Applications in Organic Synthesis. *Chem. Rev.* **2013**, *113*, 5322−5363.

(13) Goti, G.; Manal, K.; Sivaguru, J.; Dell'Amico, L. The Impact of UV Light on Synthetic Photochemistry and Photocatalysis. *Nat. Chem.* **2024**, *16*, 684−692.

(14) Chan, A. Y.; Perry, I. B.; Bissonnette, N. B.; Buksh, B. F.; Edwards, G. A.; Frye, L. I.; Garry, O. L.; Lavagnino, M. N.; Li, B. X.; Liang, Y.; Mao, E.; Millet, A.; Oakley, J. V.; Reed, N. L.; Sakai, H. A.; Seath, C. P.; MacMillan, D. W. C. Metallaphotoredox: The Merger of Photoredox and Transition Metal Catalysis. *Chem. Rev.* **2022**, *122*, 1485−1542.

(15) Hopkinson, M. N.; Tlahuext-Aca, A.; Glorius, F. Merging Visible Light Photoredox and Gold Catalysis. *Acc. Chem. Res.* **2016**, *49*, 2261−2272.

(16) Yoon, T. P. Photochemical Stereocontrol Using Tandem Photoredox-Chiral Lewis Acid Catalysis. *Acc. Chem. Res.* **2016**, *49*, 2307−2315.

(17) Rueping, M.; Vila, C.; Koenigs, R. M.; Poscharny, K.; Fabry, D. C. Dual Catalysis: Combining Photoredox and Lewis Base Catalysis for Direct Mannich Reactions. *Chem. Commun.* **2011**, *47*, 2360−2362.

(18) Barham, J. P.; König, B. Synthetic Photoelectrochemistry. *Angew. Chem., Int. Ed.* **2020**, *59*, 11732−11747.

(19) Lattke, Y. M.; Corbin, D. A.; Sartor, S. M.; McCarthy, B. G.; Miyake, G. M.; Damrauer, N. H. Interrogation of O-ATRP Activation Conducted by Singlet and Triplet Excited States of Phenoxazine Photocatalysts. *J. Phys. Chem. A* **2021**, *125*, 3109−3121.

https://doi.org/10.1021/acs.accounts.4c00847
Acc. Chem. Res. 2025, 58, 1581−1595

(20) Plutschack, M. B.; Pieber, B.; Gilmore, K.; Seeberger, P. H. The Hitchhiker's Guide to Flow Chemistry. *Chem. Rev.* **2017**, *117*, 11796−11893.
(21) Corbin, D. A.; Miyake, G. M. Photoinduced Organocatalyzed Atom Transfer Radical Polymerization (O-ATRP): Precision Polymer Synthesis Using Organic Photoredox Catalysis. *Chem. Rev.* **2022**, *122*, 1830−1874.
(22) Romero, N. A.; Nicewicz, D. A. Organic Photoredox Catalysis. *Chem. Rev.* **2016**, *116*, 10075−10166.
(23) Lee, Y.; Kwon, M. S. Emerging Organic Photoredox Catalysts for Organic Transformations. *Eur. J. Org. Chem.* **2020**, *2020*, 6028−6043.
(24) Wu, C.; Corrigan, N.; Lim, C.-H.; Liu, W.; Miyake, G.; Boyer, C. Rational Design of Photocatalysts for Controlled Polymerization: Effect of Structures on Photocatalytic Activities. *Chem. Rev.* **2022**, *122*, 5476−5518.
(25) Shao, W.; Kim, J. Metal-Free Organic Phosphors toward Fast and Efficient Room-Temperature Phosphorescence. *Acc. Chem. Res.* **2022**, *55*, 1573−1585.
(26) Uoyama, H.; Goushi, K.; Shizu, K.; Nomura, H.; Adachi, C. Highly Efficient Organic Light-Emitting Diodes from Delayed Fluorescence. *Nature* **2012**, *492*, 234−238.
(27) Parker, C. A. Phosphorescence and Delayed Fluorescence from Solutions. *Adv. Photochem.* **1964**, *2*, 305−383.
(28) Bryden, M. A.; Zysman-Colman, E. Organic Thermally Activated Delayed Fluorescence (TADF) Compounds Used in Photocatalysis. *Chem. Soc. Rev.* **2021**, *50*, 7587−7680.
(29) Dos Santos, J. M.; Hall, D.; Basumatary, B.; Bryden, M.; Chen, D.; Choudhary, P.; Comerford, T.; Crovini, E.; Danos, A.; De, J.; Diesing, S.; Fatahi, M.; Griffin, M.; Gupta, A. K.; Hafeez, H.; Hämmerling, L.; Hanover, E.; Haug, J.; Heil, T.; Karthik, D.; Kumar, S.; Lee, O.; Li, H.; Lucas, F.; Mackenzie, C. F. R.; Mariko, A.; Matulaitis, T.; Millward, F.; Olivier, Y.; Qi, Q.; Samuel, I. D. W.; Sharma, N.; Si, C.; Spierling, L.; Sudhakar, P.; Sun, D.; Tankelevičiūtė, E.; Tonet, M. D.; Wang, J.; Wang, T.; Wu, S.; Xu, Y.; Zhang, L.; Zysman-Colman, E. The Golden Age of Thermally Activated Delayed Fluorescence Materials: Design and Exploitation. *Chem. Rev.* **2024**, *124*, 13736−14110.
(30) Luo, J.; Zhang, J. Donor-Acceptor Fluorophores for Visible-Light-Promoted Organic Synthesis: Photoredox/Ni Dual Catalytic C(Sp3)-C(Sp2) Cross-Coupling. *ACS Catal.* **2016**, *6*, 873−877.
(31) Speckmeier, E.; Fischer, T. G.; Zeitler, K. A Toolbox Approach to Construct Broadly Applicable Metal-Free Catalysts for Photoredox Chemistry: Deliberate Tuning of Redox Potentials and Importance of Halogens in Donor-Acceptor Cyanoarenes. *J. Am. Chem. Soc.* **2018**, *140*, 15353−15365.
(32) Song, Y.; Kim, Y.; Noh, Y.; Singh, V. K.; Behera, S. K.; Abudulimu, A.; Chung, K.; Wannemacher, R.; Gierschner, J.; Lüer, L.; Kwon, M. S. Organic Photocatalyst for Ppm-Level Visible-Light-Driven Reversible Addition-Fragmentation Chain-Transfer (RAFT) Polymerization with Excellent Oxygen Tolerance. *Macromolecules* **2019**, *52*, 5538−5545.
(33) Back, J.; Kwon, Y.; Cho, H.; Lee, H.; Ahn, D.; Kim, H.; Yu, Y.; Kim, Y.; Lee, W.; Kwon, M. S. Visible Light Curable Acrylic Resins toward UV-light Blocking Adhesives for Foldable Displays. *Adv. Mater.* **2023**, *35*, 2204776.
(34) Kim, D.; Kim, H.; Jeon, W.; Kim, H. J.; Choi, J.; Kim, Y.; Kwon, M. S. Ultraviolet Light Debondable Optically Clear Adhesives for Flexible Displays through Efficient Visible-Light Curing. *Adv. Mater.* **2024**, *36*, 2309891.
(35) Hwang, D.; Jeon, W.; Lee, S.; Onoue, S.; Hwang, H. D.; Gierschner, J.; Kwon, M. S. A Multicomponent Visible-Light Initiating System for Rapid and Deep Photocuring through UV-Opaque Polyimide Films. *ACS Appl. Polym. Mater.* **2025**, *7*, 1741−1751.
(36) Min, H.; Kwon, Y.; Shin, S.; Choi, M.; Mehra, M. K.; Jeon, W.; Kwon, M. S.; Lee, C. W. Tailoring the Degradation of Cyanoarene-Based Photocatalystsfor Enhanced Visible-Light-Driven Halogen Atom Transfer. *Angew. Chem., Int. Ed.* **2024**, *63*, No. e202406880.
(37) Fors, B. P.; Hawker, C. J. Control of a Living Radical Polymerization of Methacrylates by Light. *Angew. Chem., Int. Ed.* **2012**, *51*, 8850−8853.
(38) Treat, N. J.; Sprafke, H.; Kramer, J. W.; Clark, P. G.; Barton, B. E.; Read de Alaniz, J.; Fors, B. P.; Hawker, C. J. Metal-Free Atom Transfer Radical Polymerization. *J. Am. Chem. Soc.* **2014**, *136*, 16096−16101.
(39) Miyake, G. M.; Theriot, J. C. Perylene as an Organic Photocatalyst for the Radical Polymerization of Functionalized Vinyl Monomers through Oxidative Quenching with Alkyl Bromides and Visible Light. *Macromolecules* **2014**, *47*, 8255−8261.
(40) Theriot, J. C.; Lim, C. H.; Yang, H.; Ryan, M. D.; Musgrave, C. B.; Miyake, G. M. Organocatalyzed Atom Transfer Radical Polymerization Driven by Visible Light. *Science* **2016**, *352*, 1082−1086.
(41) Pan, X.; Lamson, M.; Yan, J.; Matyjaszewski, K. Photoinduced Metal-Free Atom Transfer Radical Polymerization of Acrylonitrile. *ACS Macro Lett.* **2015**, *4*, 192−196.
(42) Zhou, H.; Zhang, L.; Wen, P.; Zhou, Y.; Zhao, Y.; Zhao, Q.; Gu, Y.; Bai, R.; Chen, M. Initiator-Activation Strategy-Enabled Organocatalyzed Reversible-Deactivation Radical Polymerization Driven by Light. *Angew. Chem., Int. Ed.* **2023**, *62*, No. e202304461.
(43) Sartor, S. M.; McCarthy, B. G.; Pearson, R. M.; Miyake, G. M.; Damrauer, N. H. Exploiting Charge-Transfer States for Maximizing Intersystem Crossing Yields in Organic Photoredox Catalysts. *J. Am. Chem. Soc.* **2018**, *140*, 4778−4781.
(44) McCarthy, B. G.; Pearson, R. M.; Lim, C. H.; Sartor, S. M.; Damrauer, N. H.; Miyake, G. M. Structure-Property Relationships for Tailoring Phenoxazines as Reducing Photoredox Catalysts. *J. Am. Chem. Soc.* **2018**, *140*, 5088−5101.
(45) Swisher, N. A.; Corbin, D. A.; Miyake, G. M. Synthesis, Characterization, and Reactivity of N-Alkyl Phenoxazines in Organocatalyzed Atom Transfer Radical Polymerization. *ACS Macro Lett.* **2021**, *10*, 453−459.
(46) Cole, J. P.; Federico, C. R.; Lim, C. H.; Miyake, G. M. Photoinduced Organocatalyzed Atom Transfer Radical Polymerization Using Low Ppm Catalyst Loading. *Macromolecules* **2019**, *52*, 747−754.
(47) Corbin, D. A.; Puffer, K. O.; Chism, K. A.; Cole, J. P.; Theriot, J. C.; McCarthy, B. G.; Buss, B. L.; Lim, C. H.; Lincoln, S. R.; Newell, B. S.; Miyake, G. M. Radical Addition to N, N-Diaryl Dihydrophenazine Photoredox Catalysts and Implications in Photoinduced Organocatalyzed Atom Transfer Radical Polymerization. *Macromolecules* **2021**, *54*, 4507−4516.
(48) Su, X.; Jessop, P. G.; Cunningham, M. F. Versatility of Organocatalyzed Atom Transfer Radical Polymerization and CO2-Switching for Preparing Both Hydrophobic and Hydrophilic Polymers with the Recycling of a Photocatalyst. *Macromolecules* **2019**, *52*, 6725−6733.
(49) Buss, B. L.; Lim, C. H.; Miyake, G. M. Dimethyl Dihydroacridines as Photocatalysts in Organocatalyzed Atom Transfer Radical Polymerization of Acrylate Monomers. *Angew. Chem., Int. Ed.* **2020**, *59*, 3209−3217.
(50) Bortolato, T.; Simionato, G.; Vayer, M.; Rosso, C.; Paoloni, L.; Benetti, E. M.; Sartorel, A.; Lebœuf, D.; Dell'Amico, L. The Rational Design of Reducing Organophotoredox Catalysts Unlocks Proton-Coupled Electron-Transfer and Atom Transfer Radical Polymerization Mechanisms. *J. Am. Chem. Soc.* **2023**, *145*, 1835−1846.
(51) Huang, Z.; Gu, Y.; Liu, X.; Zhang, L.; Cheng, Z.; Zhu, X. Metal-Free Atom Transfer Radical Polymerization of Methyl Methacrylate with Ppm Level of Organic Photocatalyst. *Macromol. Rapid Commun.* **2017**, *38*, 1600461.
(52) Ma, Q.; Song, J.; Zhang, X.; Jiang, Y.; Ji, L.; Liao, S. Metal-Free Atom Transfer Radical Polymerization with Ppm Catalyst Loading under Sunlight. *Nat. Commun.* **2021**, *12*, 429.
(53) Shao, H.; Li, S.; Jiang, Y.; Song, J.; Zhang, X.; Chen, J.; Liao, S. Sulfur-Doped Anthanthrenes as Effective Organic Photocatalysts for Metal-Free ATRP and PET-RAFT Polymerization under Blue and Green Light. *Polym. Chem.* **2024**, *15*, 4134−4140.

https://doi.org/10.1021/acs.accounts.4c00847
Acc. Chem. Res. 2025, 58, 1581−1595

(54) Xu, J.; Jung, K.; Atme, A.; Shanmugam, S.; Boyer, C. A Robust and Versatile Photoinduced Living Polymerization of Conjugated and Unconjugated Monomers and Its Oxygen Tolerance. *J. Am. Chem. Soc.* **2014**, *136*, 5508−5519.
(55) Lee, Y.; Boyer, C.; Kwon, M. S. Photocontrolled RAFT Polymerization: Past, Present, and Future. *Chem. Soc. Rev.* **2023**, *52*, 3035−3097.
(56) Chen, M.; Zhong, M.; Johnson, J. A. Light-Controlled Radical Polymerization: Mechanisms, Methods, and Applications. *Chem. Rev.* **2016**, *116*, 10167−10211.
(57) Zhang, Z.; Corrigan, N.; Bagheri, A.; Jin, J.; Boyer, C. A Versatile 3D and 4D Printing System through Photocontrolled RAFT Polymerization. *Angew. Chem., Int. Ed.* **2019**, *58*, 17954−17963.
(58) Ma, F.; Luo, Z. M.; Wang, J. W.; Ouyang, G. Highly Efficient, Noble-Metal-Free, Fully Aqueous CO_2 Photoreduction Sensitized by a Robust Organic Dye. *J. Am. Chem. Soc.* **2024**, *146*, 17773−17783.
(59) Dadashi-Silab, S.; Atilla Tasdelen, M.; Mohamed Asiri, A.; Bahadar Khan, S.; Yagci, Y. Photoinduced Atom Transfer Radical Polymerization Using Semiconductor Nanoparticles. *Macromol. Rapid Commun.* **2014**, *35*, 454−459.
(60) Kütahya, C.; Schmitz, C.; Strehmel, V.; Yagci, Y.; Strehmel, B. Near-Infrared Sensitized Photoinduced Atom-Transfer Radical Polymerization (ATRP) with a Copper(II) Catalyst Concentration in the Ppm Range. *Angew. Chem., Int. Ed.* **2018**, *57*, 7898−7902.
(61) Dadashi-Silab, S.; Lorandi, F.; DiTucci, M. J.; Sun, M.; Szczepaniak, G.; Liu, T.; Matyjaszewski, K. Conjugated Cross-Linked Phenothiazines as Green or Red Light Heterogeneous Photocatalysts for Copper-Catalyzed Atom Transfer Radical Polymerization. *J. Am. Chem. Soc.* **2021**, *143*, 9630−9638.
(62) Sobieski, J.; Gorczyński, A.; Jazani, A. M.; Yilmaz, G.; Matyjaszewski, K. Better Together: Photoredox/Copper Dual Catalysis in Atom Transfer Radical Polymerization. *Angew. Chem., Int. Ed.* **2025**, *64*, No. e202415785.
(63) Szczepaniak, G.; Fu, L.; Jafari, H.; Kapil, K.; Matyjaszewski, K. Making ATRP More Practical: Oxygen Tolerance. *Acc. Chem. Res.* **2021**, *54*, 1779−1790.
(64) Ghosh, I.; Ghosh, T.; Bardagi, J. I.; König, B. Reduction of Aryl Halides by Consecutive Visible Light-Induced Electron Transfer Processes. *Science* **2014**, *346*, 725−728.
(65) Chernowsky, C. P.; Chmiel, A. F.; Wickens, Z. K. Electrochemical Activation of Diverse Conventional Photoredox Catalysts Induces Potent Photoreductant Activity. *Angew. Chem., Int. Ed.* **2021**, *60*, 21418−21425.
(66) Beatty, J. W.; Stephenson, C. R. J. Amine Functionalization via Oxidative Photoredox Catalysis: Methodology Development and Complex Molecule Synthesis. *Acc. Chem. Res.* **2015**, *48*, 1474−1484.
(67) Villa, M.; Fermi, A.; Calogero, F.; Wu, X.; Gualandi, A.; Cozzi, P. G.; Troisi, A.; Ventura, B.; Ceroni, P. Organic Super-Reducing Photocatalysts Generate Solvated Electrons via Two Consecutive Photon Induced Processes. *Chem. Sci.* **2024**, *15*, 14739−14745.
(68) Min, H.; Kwon, Y.; Shin, S.; Choi, M.; Mehra, M. K.; Jeon, W.; Kwon, M. S.; Lee, C. W. Tailoring the Degradation of Cyanoarene-Based Photocatalystsfor Enhanced Visible-Light-Driven Halogen Atom Transfer. *Angew. Chem., Int. Ed.* **2024**, *63*, No. e202406880.
(69) Constantin, T.; Zanini, M.; Regni, A.; Sheikh, N. S.; Juliá, F.; Leonori, D. Aminoalkyl Radicals as Halogen-Atom Transfer Agents for Activation of Alkyl and Aryl Halides. *Science* **2020**, *367*, 1021−1026.
(70) Glaser, F.; Kerzig, C.; Wenger, O. S. Multi-Photon Excitation in Photoredox Catalysis: Concepts, Applications, Methods. *Angew. Chem., Int. Ed.* **2020**, *59*, 10266−10284.
(71) Ko, H. M.; Lee, C. W.; Kwon, M. S. Degradation Behavior of Donor-acceptor Cyanoarenes-based Organic Photocatalysts. *ChemCatChem.* **2023**, *15*, No. e202300661.
(72) Lalevée, J.; Telitel, S.; Xiao, P.; Lepeltier, M.; Dumur, F.; Morlet-Savary, F.; Gigmes, D.; Fouassier, J. P. Metal and Metal-Free Photocatalysts: Mechanistic Approach and Application as Photoinitiators of Photopolymerization. *Beilstein J. Org. Chem.* **2014**, *10*, 863−876.
(73) Dietlin, C.; Schweizer, S.; Xiao, P.; Zhang, J.; Morlet-Savary, F.; Graff, B.; Fouassier, J. P.; Lalevée, J. Photopolymerization upon LEDs: New Photoinitiating Systems and Strategies. *Polym. Chem.* **2015**, *6*, 3895−3912.
(74) Chen, H.; Noirbent, G.; Zhang, Y.; Brunel, D.; Gigmes, D.; Morlet-Savary, F.; Graff, B.; Xiao, P.; Dumur, F.; Laleveé, J. Novel D-π-A and A-π-D-π-A Three-Component Photoinitiating Systems Based on Carbazole/Triphenylamino Based Chalcones and Application in 3D and 4D Printing. *Polym. Chem.* **2020**, *11*, 6512−6528.
(75) Stafford, A.; Ahn, D.; Raulerson, E. K.; Chung, K. Y.; Sun, K.; Cadena, D. M.; Forrister, E. M.; Yost, S. R.; Roberts, S. T.; Page, Z. A. Catalyst Halogenation Enables Rapid and Efficient Polymerizations with Visible to Far-Red Light. *J. Am. Chem. Soc.* **2020**, *142*, 14733−14742.
(76) Uddin, A.; Allen, S. R.; Rylski, A. K.; O'Dea, C. J.; Ly, J. T.; Grusenmeyer, T. A.; Roberts, S. T.; Page, Z. A. Do The Twist: Efficient Heavy-Atom-Free Visible Light Polymerization Facilitated by Spin-Orbit Charge Transfer Inter-System Crossing. *Angew. Chem., Int. Ed.* **2023**, *62*, No. e202219140.
(77) Ahn, D.; Stevens, L. M.; Zhou, K.; Page, Z. A. Rapid High-Resolution Visible Light 3D Printing. *ACS Cent. Sci.* **2020**, *6*, 1555−1563.
(78) Sprick, E.; Becht, J. M.; Graff, B.; Salomon, J. P.; Tigges, T.; Weber, C.; Lalevée, J. New Hydrogen Donors for Amine-Free Photoinitiating Systems in Dental Materials. *Dent. Mater.* **2021**, *37*, 382−390.

https://doi.org/10.1021/acs.accounts.4c00847
Acc. Chem. Res. 2025, 58, 1581−1595